EERA DTOC

THE EUROPEAN ENERGY RESEARCH ALLIANCE
DESIGN TOOLS FOR OFFSHORE WIND FARM CLUSTER

Benchmark report on wake models at the cluster scale

Jake Badger, Pedro Angel Jimenez Muñoz, Pedro Miguel Fernandes Correia, Sergio Lozano Galiana, Patrick Volker, John Prospathopoulos, Alexis Mouche, Merete Badger, Gerard Schepers, Ana Maria Palomares Losada, Jorge Navarro Montesinos, Ivan Moya Mallafre, Kurt Hansen, Charlotte Bay Hasager

August 13, 2013

Agreement n.:	FP7-ENERGY-2011-1/ n°282797
Duration	January 2012 to June 2015
Co-ordinator:	DTU Wind Energy, Risø Campus, Denmark

Support by:

SEVENTH FRAMEWORK PROGRAMME

PROPRIETARY RIGHTS STATEMENT

This document contains information, which is proprietary to the "EERA-DTOC" Consortium. Neither this document nor

Document information

Document Name:	Benchmark report on wake models at the cluster scale
Document Number:	D1.4
Author:	Jake Badger, Pedro Angel Jimenez Muñoz, Pedro Miguel Fernandes Correia, Sergio Lozano Galiana, Patrick Volker, John Prospathopoulos, Alexis Mouche, Merete Badger, Gerard Schepers, Ana Maria Palomares Losada, Jorge Navarro Montesinos, Ivan Moya Mallafre, Kurt Hansen, Charlotte Bay Hasager
Date:	August 13, 2013
WP:	WP1
Task:	T1.4

Table of contents

1 EXECUTIVE SUMMARY 4

2 INTRODUCTION 5

3 ECN FARMFLOW MODEL 6

4 DTU WIND ENERGY MESOSCALE MODELLING 7
4.1 Idealized simulations with WRF-EWP 7
4.2 Mesoscale wind farm wake parameterization based on microscale modelling output 7

5 CIEMAT 11
5.1 Mesoscale modelling using the WRF wind farm parameterization 11
5.2 Influence on modelled wake wind speed time series at neighbouring farm 13

6 CENER METHODOLOGY: 17
6.1 Skiron Model Configuration: 17
6.2 WRF Model Configuration: 19
6.3 Mesoscale model sensitivity test: 19

6.3.1 WRF-ARW 19

6.3.2 Horns Rev Results by sector 22

6.3.3 SKIRON 22
6.4 SKIRON Test Cases 22

7 CLS AND DTU WIND ENERGY – SATELLITE DATA ANALYSIS 26
7.1 Visual indications of wakes (qualitative), including identification of meandering. 26
7.2 Analysis of single scenes, using 3 parallel transects 29
7.3 Climatological (averaged) analysis of wind farm wakes 32

8 SYNTHESIS AND DISCUSSION 35

9 SUMMARY AND CONCLUSIONS 37

10 REFERENCES: 38

1 EXECUTIVE SUMMARY

This report describes a range of approaches to model wind farm wakes at cluster scale. This scale calls for the application of atmospheric mesoscale models. The approaches outlined in the report describe application of two different mesoscale models (WRF and SKIRON) in two different modelling frameworks (idealized and realistic) The influence that the wind turbines exert in the resolved atmospheric flow is represented using three different methods: 1) The wind turbines are represented by increasing the surface roughness; 2) The wind turbines constitute an elevated sink of momentum and a source of turbulent kinetic energy and; 3) A novel approach developed within the framework of the project that represents the wind turbines as an elevated sink of momentum allowing for a vertical expansion of the wake The performance of these approaches is tested with observations of the wind and power production recorded at the Horns Rev I wind farm. In addition, results are compared with the simulation from a microscale model (FarmFlow) in order to provide some insight of the performance of a usual approach to obtain high spatial resolution of the wake structure. On the basis of the realistic simulation of the wake effects by the mesoscale models, the influence of wakes from hypothetical or future large offshore wind farms within a cluster is also examined.

Wake images derived from satellite borne synthetic aperture radar (SAR) wind speed data are used to assess the realism of some aspects of the simulated wakes. A number of SAR analysis methods are described. The SAR data is highly valuable in providing spatial coverage of the wind speed field on scales appropriate for mesoscale modelling.

The different wake modelling approaches are in broad agreement providing similar results that the microscale approach under neutral atmospheric conditions. The simulations tend to underestimate the wind speed deficit associated with the wake near the wind farm (less than 4 km downstream). There is a better agreement between the models and observations at larger downstream distances (more than 4 km). This indicates that mesoscale simulations have potential to model the impacts that large offshore wind farms within a cluster exert among each other. In this direction, results indicate that dynamical impact of wind farm wakes moving on to neighbouring downstream wind farms may add considerable variability to wind farm production. This is an area of interest for continued investigation.

Validation of the mesoscale modelling approaches, as described within this report, is certainly underway, however it is highlighted that more validation, across a large range of meteorological conditions is still required. These validation exercises will require the availability and careful analysis of more wind farm wake data. Especially valuable is data at a number of kilometres from the wind farm, i.e. more than 5 km, to analyze the length and intensity of the wakes. It is expected that the LIDAR measurement campaign associated with DTOC will be of particular interest as it will provide a more extended vertical structure of the wind conditions than data from meteorological towers covering some of the scales relevant for mesoscale modelling.

2 INTRODUCTION

The purpose of this report is to describe the work undertaken within the WP 1.2. The bench marking consists of describing a number of modelling methods to estimate the wind speed and wind power deficits associated with wind farm wakes, outlining the methods' properties, strengths and weaknesses, and perform, where possible, validation against observations. The validation makes use of measurements collected at wind farms and prepared within the framework of this project, (Hansen, 2013), and remote sensing data from satellite borne instruments (SAR). More information about the measurement data can be found in **D1.1 Basic data for testing of mesoscale and coupled use**.

From a very general perspective, there are two main types of wake models. There are models which resolve individual wakes from a number of turbines, see **D1.3 Benchmark report on wake models at wind farm scale**. These models operate at rather fine spatial resolution, on the order of metres, and thus are called microscale models. There are also models which simulate the collective impact of multiple wakes from several wind turbines. These are used in mesoscale models, typically run at horizontal resolutions of thousands/hundreds of meters, and thus are called mesocale wake models. For example the Weather Research and Forecasting model (WRF, Skamarock et al. 2008), has recently incorporated a parameterization to represent the drag exerted by wind turbines. The cross-cover of information provided by the microscale to the mesoscale models is beginning to developed, and is described in **D1.2 Report on physical scale integration (coupled use)**. The application of this new development is also given in this report. Although mesoscale models usually simulate collectively the wind turbines, increasing computational resources make possible simulation at high enough spatial resolution such that a single mesoscale grid cell contains a single turbine, as we will see herein. In spite of this, there is a marked difference between the modelling of the turbine wake which has scales much smaller than what can be resolved by the mesoscale model.

Other differences between the microscale and mesoscale approaches are the extension of the region where the atmospheric evolution is modelled and the way the effects of the wind turbines are represented in the models. The microscale model domain is extended to encompass length scales normally associated with the mesoscale (hundreds/thousands of meters). Description of the microscale models is given in **D1.3 Benchmark report on wake models at wind farm scale.**

Mesoscale models simulate the atmospheric evolution over a much wider area (thousands/hundreds of km). These can use idealized simulations as a basis, or use more realistic dynamical modelling as a basis. The mesoscale modelling of wind farms can be conducted using the existing wake paramerization in WRF (Fitch et al 2012), or can use the newly developed method described in Volker et al (2013). In the WRF paramerization the wind drag exerted by the wind turbines is represented using an elevated momentum sink term which is at a time a source of turbulent kinetic energy turbulence. In the Volker et al. (2013) method, wind turbines are treated as an elevated momentum sink term, in contrast vertical wake expansion within mesoscale model grid cells is modelled and there is no source term for turbulent kinetic energy. Another method used in this work is to apply a different land use class to the area occupied by the wind farms. This method is based on representing the wind farm by increasing the surface roughness length.

The structure of the report is to take each project partner's approach in turn (Sections 2 to 6), then to discuss the remote sensing methods (Section 7) and synthesis the different methods and results (Section 8). Finally, conclusions will be stated and recommendations on the future effort and investigation given (Section 9).

3 ECN FARMFLOW MODEL

In this approach a microscale model, usually dedicated to turbine and wind farm wakes, is extended to cover mesoscales. It can be included here as a bridge between microscale modelling to the mesoscale modelling.

FarmFlow makes use of a 3D parabolized RANS model with a k-ε turbulence model for closure, based on the UPMWAKE code originally developed by Crespo et al (1985). The free stream is modelled with equations of Panofsky and Dutton (1984). Due to the parabolization of UPMWAKE, the original code is not applicable in the near wake region, where pressure gradients in flow direction are necessary to calculate the flow deceleration in the wake. To include the near wake region, FarmFlow uses a database with axisymmetric flow fields of the near wake region, which have been calculated with a free vortex wake model. From this database, the pressure gradients in the near wake region are prescribed as forces in the momentum equations. The constants of the k- ε turbulence model have been selected to match the basic flow in neutral atmospheric conditions. In the near wake region however, these coefficients are changed to match experimental results of the wake development in this region.

	Wind speed [m/s]		
Case 1	At last turbine	M6	M7
Sector width 5 degrees	6.52	7.33	7.47
Sector width 15 degrees	6.67	7.16	7.41
Sector width 30 degrees	6.77	7.01	7.42

Table 1: Results for the Horns Rev I benchmarking case from the ECN's FarmFlow model.

Table 1 gives the wind speed at the last row of turbines and at mast 6 (M6) and mast 7 (M7) at 7040 m and 11040 m from first row of turbines. It can be seen that for the last turbine, the minimum wind speed occurs for the narrowest sector width. This is because for a narrow sector the turbine is more often in the deepest part of the wake. For M6 the minimum wind speed occurs for the widest sector width. This is probably due to the slight offset of the latitudinal position of the mast compared to the column of turbines upwind. With a narrow sector, M6 is not in the deepest part of the wake developing behind the upwind column of wind turbines. Finally the wind speed at M7 is not very sensitive to the sector width. There is a small element of the feature seen at M6, namely the narrow sector giving a slightly higher wind speed.

The results from ECN's FarmFlow will be later compared with results from mesoscale modelling and satellite remote sensing measurements, and thus server as a microscale model reference.

4 DTU WIND ENERGY MESOSCALE MODELLING

Due to the large ratio between the horizontal grid spacing and the turbine blade diameter, we assume in the Explicit Wake Parameterization (EWP), that within a turbine containing grid cell the turbine caused turbulence, with a characteristic length scale of around a turbine diameter, will be balanced by its dissipation. The downstream sub-grid scale velocity deficit development is then described explicitly via a turbulence diffusion process. The velocity deficit is assumed to be approximately Gaussian shaped with a characteristic length and velocity scale. The characteristic length scale is obtained from a 1-dimensional diffusion equation and the velocity scale from the thrust equation. To the model Navier-Stokes equation we apply a grid cell average velocity deficit, which is a function of the horizontal grid spacing. The details of this new WRF parameterization are described in Volker et al (2013).

4.1 Idealized simulations with WRF-EWP

The WRF model has been used in idealised case mode to model the Horns Rev I wind farm wake for very controlled atmospheric conditions. This implies that the model is initialised with a homogeneous (dry) sounding profile, with open boundary conditions (no forcing). In our set-up a Coriolis force acts on the velocity perturbations and the surface fluxes were set to zero. This means that the model will converge to a neutral atmosphere and above the boundary layer in geostrophic balance. For the presented results here the hub height wind is 7.97 m/s westerly wind direction (269.4 degrees). Since the model was run in with dry conditions, the cloud microphysics could be switched off. For all simulations the MYNN (1.5) PBL second order turbulence diffusion scheme was used. The model was set up with 80 times 30 grid cells in the horizontal direction. In the vertical direction we used 40 layers (the lowest layers were at 10, 30, 50 ,71 and 92 m). The horizontal resolution was set to 1120 m, implying that the Horns Rev I occupied 5 times 4 grid cells with 4 turbines per grid cell.

Figure 1(a) shows the horizontal section at 70 m and vertical cross section view of the Horns Rev I wind farm wake in the idealized conditions described above (namely, a 8 m/s westerly wind). It can be seen that the wake extends downstream about 20-30 km, and extends in the vertical to about 200 m. Figure 2 (a) shows the validation of the idealized mesoscale wind farm wake simulations against measurement derived wake properties based on filtered data described in **D1.1 Basic data for testing of mesoscale and coupled use** and Hansen (2013). These results provide a control against which adaptations of the mesoscale wind farm wake parameterization are compared.

4.2 Mesoscale wind farm wake parameterization based on microscale modelling output

In connection with WP1.3 and as described in **D1.2 Report on physical scale integration (coupled use)** the WRF-EWP wake parameterization was adapted to allow for a range of different approaches using thrust information from microscale model CRESflowNS in a number of different ways. These approaches are list in Table 2.

Parameterization	Thrust calculation	Vertical thrust distribution	aggregations
WRF-EWP	thrust curve	diffusive wake expansion	meso grid aggr
WRF-CRES-EWP CRES	CRESflowNS	diffusive wake expansion	meso grid aggr.
WRF-CRES-ROTOR CRES	CRESflowNS	proportional to rotor area per level	meso grid aggr.
WRF-CRES-ROTOR-FA CRES	CRESflowNS	proportional to rotor area per level	wind farm aggr.

Table 2: Table summarizing the different wake parameterizations tested.

The two parameterizations using the diffusive vertical wake expansion, WRF-EWP and WRF-CRES-EWP (Figure 1. a and b) are rather similar. The minimum wind speed obtained is approximately 6.8 m/s in the downwind portion of the wind farm. The horizontal extent of the wake is slightly longer for WRF-EWP. The vertical profile of velocity deficit is also similar between WRF-EWP and WRF-CRES-EWP, with the 0.8 m/s deficit reaching approximately 150 m above surface level. However the WRF-EWP wake has a slightly large vertical extent.

For the two parameterizations using the vertical thrust distribution proportional to rotor swept area per level (i.e. no vertical wake expansion), WRF-CRES-ROTOR and WRF-CRES-ROTORFA, the minimum wind speed obtained is approximately 6.2 m/s and 6.0 m/s respectively. However the horizontal wake extent is shorter than for the diffusive vertical expansion parameterization. The shortest wake is for the WRF-CRES-ROTOR-FA parameterization. The vertical profile of velocity deficits are markedly different compared to WRF-EWP and WRF-CRESEWP. The deficit exceeds 1.8 m/s in both cases, a little higher in the WRF-CRES-ROTOR-FA parameterization. However, the 0.8 m/s deficit reaches only 120 m above surface level. Consistent with the neglect of a sub-grid scale vertical wake expansion, it can be seen the deficit is more concentrated in the vertical in the WRF-CRES-ROTOR and WRF-CRES-ROTOR-FA parameterizations.

The difference between the mesoscale grid aggregation and wind farm aggregations parameterizations can be assessed by comparison of the WRF-CRES-ROTOR and WRF-CRES-ROTOR-FA results. The main differences are seen in the proximity of the wind farm, but further downwind the differences are reduced. In Figure 2 the results from the mesoscale model parameterizations are compared with the measurements from the wind farm. The measurements are for wind speed within the range 7.5 – 8.5 m/s and wind direction within the range 255–285 degrees. In Figure 2 the wake wind speed deficit can be seen inside the farm at each turbine row and downstream of the wind farm at anemometers M6 and M7. Considering WRF-EWP (Figure 2a) as the reference, we can see that WRF-CRES-EWP (Figure 2b) gives a slightly smaller wake deficit. Both parameterizations show good agreement with the measurement data, and lie well within the error bars. Considering next WRF-CRES-ROTOR (Figure 2c), it can be seen that the wake deficit is large inside the wind farm, on the lower bounds of the error bars of the measurement data. Downwind of the wind farm, the difference compared to WRF-EWP is less pronounced, however the velocity deficits are still larger. Considering WRF-CRES-ROTOR-FA (Figure 2d), it can be seen that inside the wind farm the deficit is very strong, below the lower bounds of the error bar. Downwind of the wind farm the difference is much reduced and agreement with measurement at masts M6 and M7 is good.

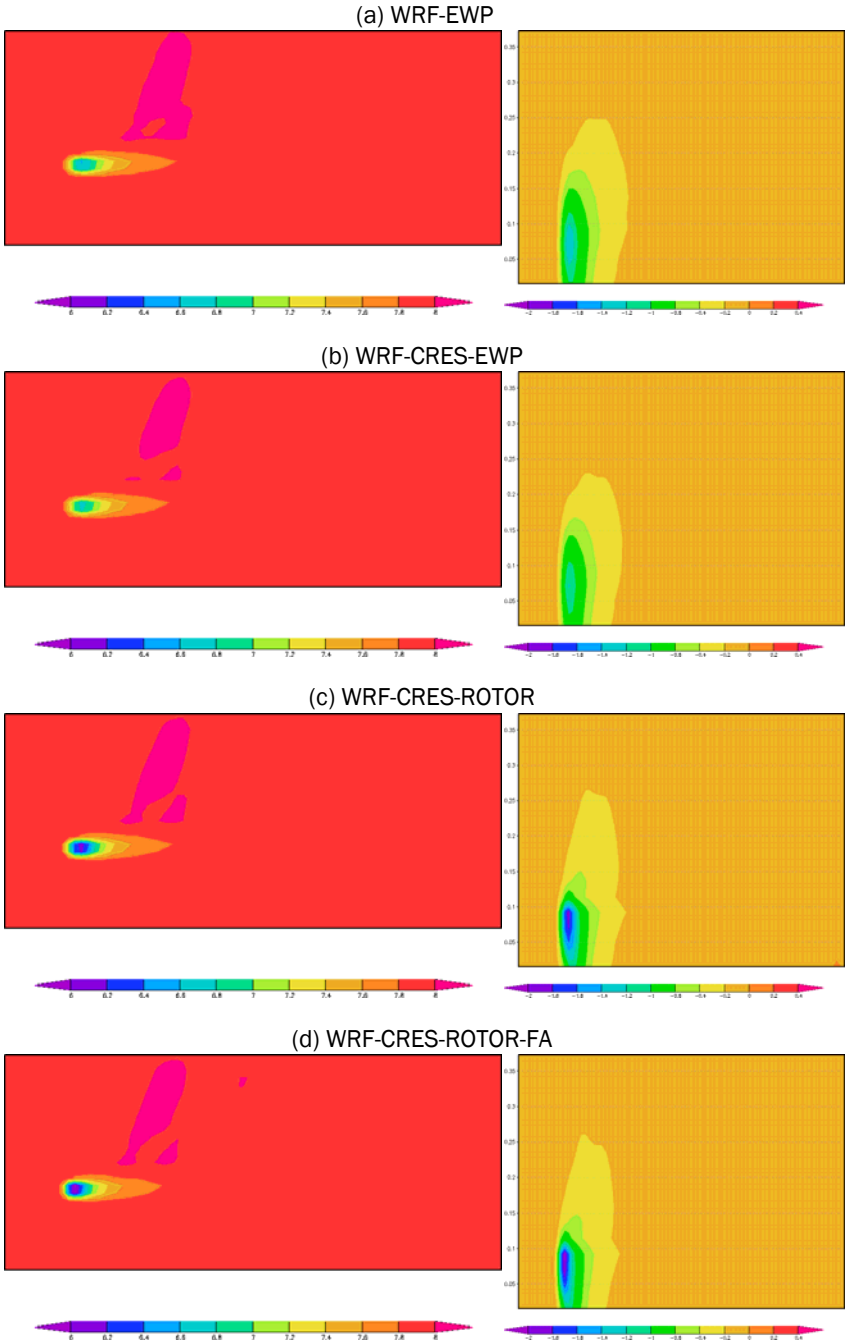

Figure 1: Plots of wind speed at 70 m showing wind farm wake (left) and vertical sections of wake velocity deficit (right) for simulations having an inflow westerly surface wind of 8 m/s using different wake parameterizations, (a) WRF-EWP, (b) WRF-CRES-EWP, (c) WRF-CRES-ROTOR (d) WRF-CRES-ROTOR-FA. The wake maps (left) show the westerly component of wind speed at 70 m above surface level. The x-axis has 180 km extent and the y-axis has 65 km extent. The vertical sections of wake velocity deficit (right) are a slice through the wind farm. The x-axis extent is 180 km, the vertical extent is from 0 – 350 m above surface level.

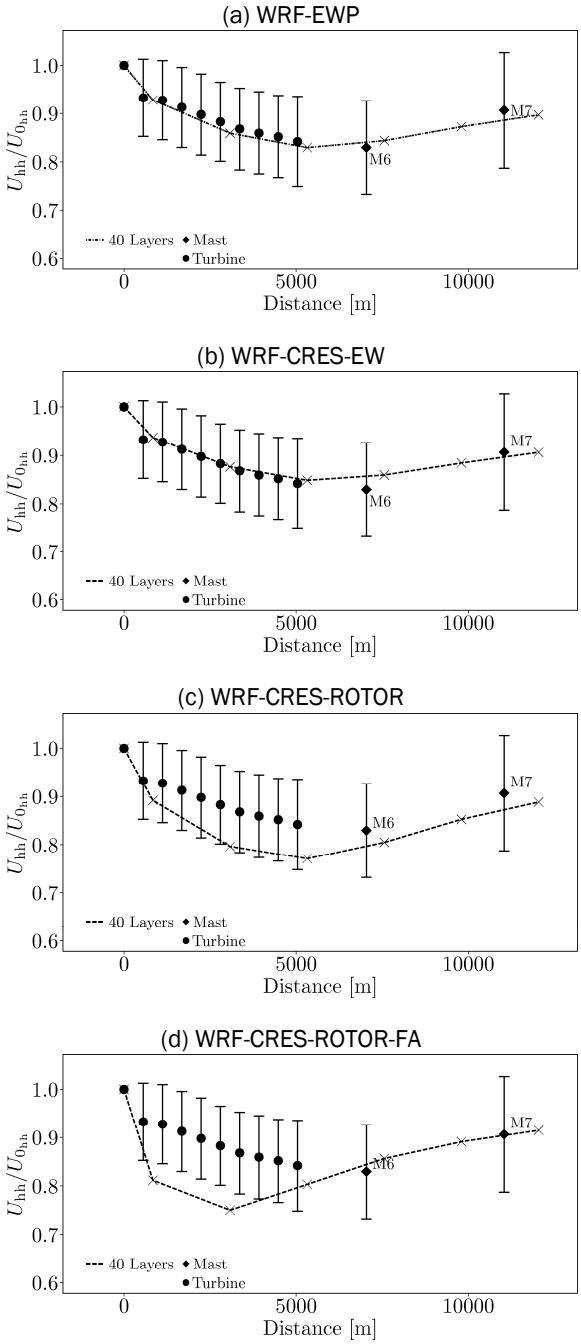

Figure 2: Recovery validation plots for different parameterizations used, (a) WRF-EWP, (b) WRF-CRES-EWP, (c) WRF-CRES and (d) WRF-CRES-FA. The x-axis is the distance in metres from the first turbine row, the y-axis is the wake horizontal wind speed expressed as a fraction of the inflow wind speed, both at 70 m above surface level, i.e. for first row turbines the value is 1. The black dots are measurements based on wind turbine power or from anemometers at mast 6 (M6) and mast (M7) downwind of the wind farm.

5 CIEMAT

Two interrelated exercises were performed based on dynamical simulations using the mesoscale approach. The first one consists of the first comprehensive evaluation of the WRF wind farm parameterization ability to reproduce the wind and wind power deficits within a wind farm (Jimenez et al. 2013). The second one inspects the downstream effects of an isolated wind farm and a cluster of wind farms.

During the evaluation, the ability of the WRF wind farm parameterization (Fitch et al. 2012) to reproduce the effects of the wind turbines in the atmospheric evolution has been tested for the first time in a real offshore environment. The evaluation was performed at the Horns Rev wind farm. It combines 3 years of *in situ* observations (Hansen 2013), and WRF simulations spanning the same temporal period (2005 – 2007) at a high horizontal resolution of 333 m over the wind farm. This is the first comprehensive comparison of the wind farm parameterization performance against observations, when run in a realistic way.

The downstream effects of the wind farms were inspected over Horns Rev as well as in a future cluster of wind farms over the German Bight. The downstream effects were examined using the WRF mesoscale model. The experiment builds on the realistic simulation of the wakes found during the evaluation. A more complete description of both studies is presented in the following subsections.

5.1 Mesoscale modelling using the WRF wind farm parameterization

The WRF mesoscale model (Skamarock et al. 2008) has recently incorporated the possibility of modelling the effects that the wind turbines exert over the atmospheric evolution. The turbines are represented by assuming that they constitute an elevated sink of momentum and a source of turbulent kinetic energy. The parameterization is described in Fitch et al. 2012. That article examines the effects that an idealized offshore wind farm produce over the atmospheric evolution. The study compared two idealized WRF runs with and without parameterizing the wind farm effects to test model sensitivities.

The evaluation performed by CIEMAT uses the observational dataset described in Hansen (2013). The dataset consists of a total of three years (2005 – 2008) of wind and wind power records at Horns Rev. The WRF simulations span the same 3 years of the observational dataset. The evaluation compares sub-samples with equivalent atmospheric conditions from the observational and simulated datasets in order to inspect the performance of the parameterization in a range of atmospheric states. The following lines provide a brief summary of main results. A more complete description of the evaluation is described in Jimenez et al (2013) where the interested reader is referred to for specific details.

The initial and boundary conditions necessary to run a limited area model like WRF were obtained from the ERA-Interim reanalysis project (Dee et al. 2011). The horizontal resolution of the ERA-interim data is 0.75 x 0.75 degrees. Reanalysis products blend modelling with observations in what we can consider our best estimation of the atmospheric state. Hence, we are testing the performance of the WRF model in a real environment. A total of 5 domains were used to progressively increase the spatial resolution of the atmospheric evolution over Horns Rev. Figure 3 shows the area covered by the different domains. Domain 1 has a horizontal resolution of 27 km, domain 2 uses 9 km, domain 3 has 3 km, domain 4 has 1 km, and, finally, domain 5 has a horizontal resolution of 333 m. This high spatial resolution in the innermost domain was necessary to resolve the individual wind turbines in the simulation (Figure 4).

The evaluation indicated that although WRF underestimates the wind and wind power deficits within the wind farm, it is able to reproduce a realistic response to different atmospheric conditions. Two illustrative examples are herein provided.

Figure 5 Figure 6 show the wind and wind power deficits as a function of the direction of the flow and the atmospheric stability, respectively. In both cases, the wind speed at the hub height (70 m) is 8 m/s and the turbulence intensity is 7%. The power deficit at a given turbine (Pturb) is calculated with respect to an unperturbed one (Pref) according to Pdeficit=1-Pturb/Pref. There is a

large power deficit from the first to the second column of wind turbines and this is reproduced by WRF. Departures from the western direction lead to a reduction of the deficits which is also qualitatively reproduced by the mesoscale simulation (Figure 5). The tendencies of the wind and wind power deficits to the atmospheric stability are also qualitatively reproduced by WRF (Figure 6).

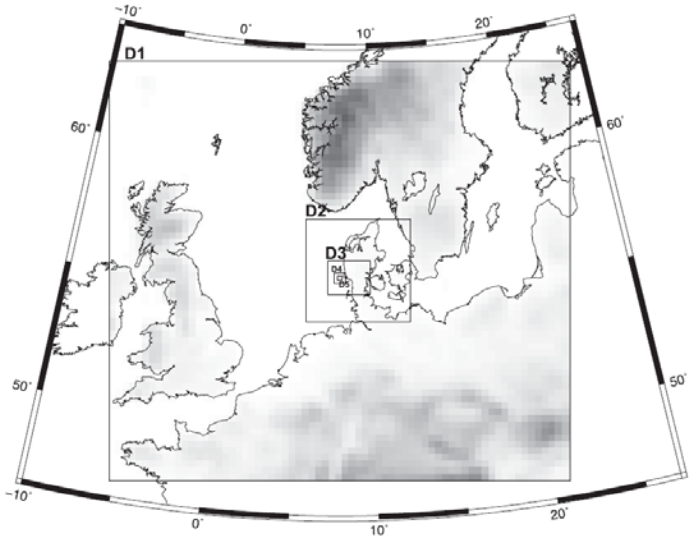

Figure 3: WRF calculation domains, indicating the 5 calculation domains used.

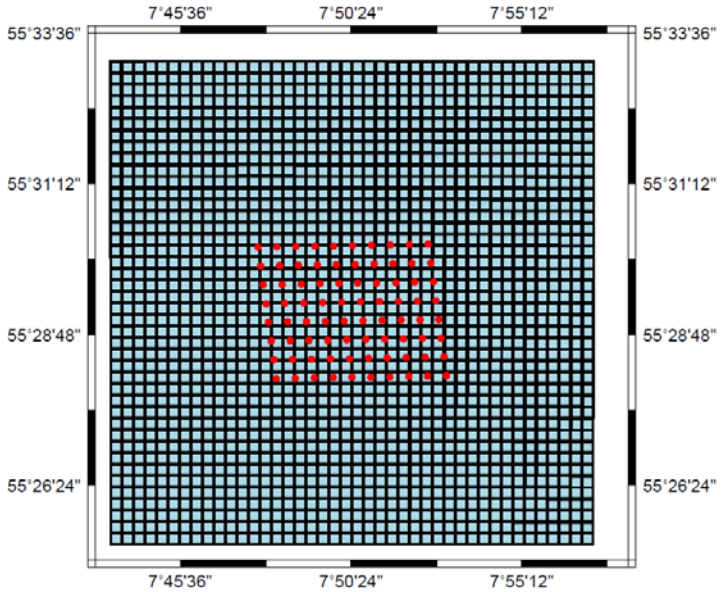

Figure 4: The inner domain of the WRF simulations (squares) and the wind turbines of the Horns Rev wind farm (red circles).

The underestimation of the wind speed deficit is at least partially associated with the way the turbines' thrust coefficient and power coefficients are represented in the model. WRF uses an empirical formula to calculate the thrust and power coefficients. This formula underestimates the thurst coefficient of the wind turbines at Horns Rev I by about 0.1 for wind speeds of 8 m/s which in turn will underestimate the drag exerted by the turbines. Preliminary simulations replacing the coefficients with those provided by the manufacturer point in this direction. In addition, Volker et al. (2013) found that replacing the empirical relationship with actual turbine thrust curve information increases the thrust and the wake effects in idealized WRF simulations.

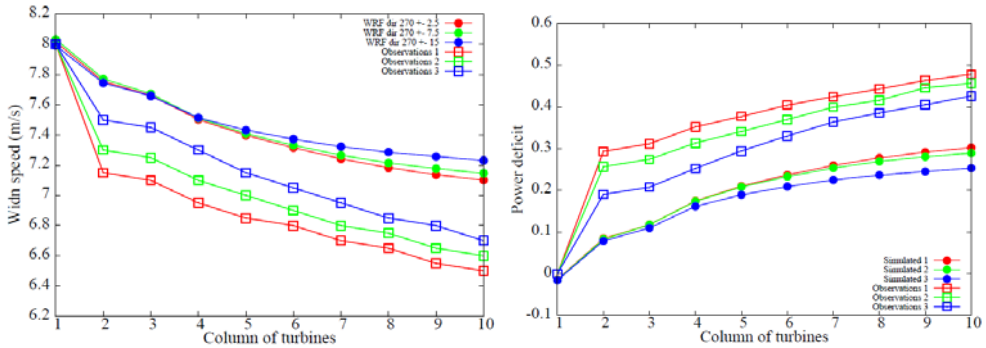

Figure 5: Results from WRF simulations filtered according to Hansen (2013) for case 1.

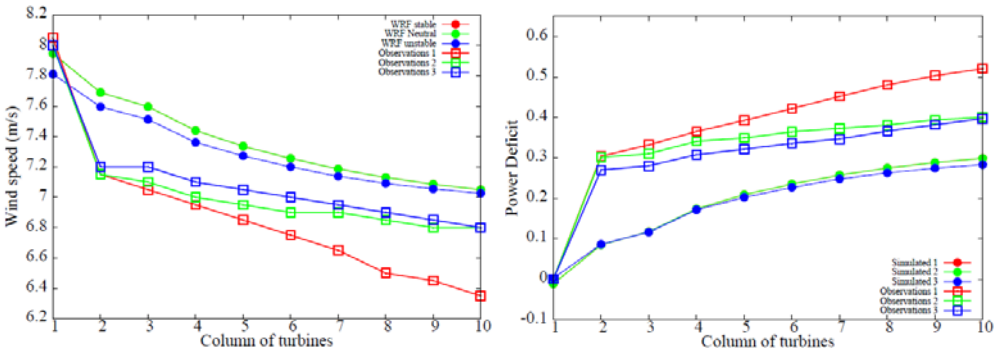

Figure 6: Results from WRF simulations filtered according to Hansen (2013) for case 2.

5.2 Influence on modelled wake wind speed time series at neighbouring farm

Although the WRF model underestimates the wind/wind power deficits generated by the wind turbines, it is able to produce a realistic response for the wakes associated with the different atmospheric conditions (Figure 5 andFigure 6). This encouraged us to explore the downstream effects produced by the 80 turbines of the Horns Rev wind farm and by a future cluster of wind farms over German Bight with 531 turbines.

Figure 7 shows the mean wind speed at the hub height for the cases with neutral stability and western winds from the atmospheric evolution at domain 4 (1 km of horizontal resolution, Figure 3). The effects of the wind farm are noticeable 15 km downstream. WRF underestimates the wind farm wakes which suggests that the downstream effects of the wind farm are likely to be noticeable at further distances. Hence, 15 km can be considered as a lower limit to the distance between large wind farms within a cluster if no wake perturbation among them is desired.

The potential influence that different wind farms may exert over each other in a real cluster of wind farms was also examined. For this purpose, potential downstream effects of the wind farm wakes were inspected over a future cluster over German Bight. The cluster is shown in Figure 8 (red dots). There will be a total of 531 wind turbines in a small area of about 90 km by 70 km. The wind farms are located relatively close to each other so downstream effects associated with wakes would not be surprising. For instance, the reference wind farm highlighted with a blue cross in Figure 8 is only 8 km apart from the wind farm located to the west. Keeping in mind the results over Horns Rev (Figure 7) the effects of this wind farm over the reference one would be noticeable. To explore this possibility a sensitivity experiment with the WRF model was performed.

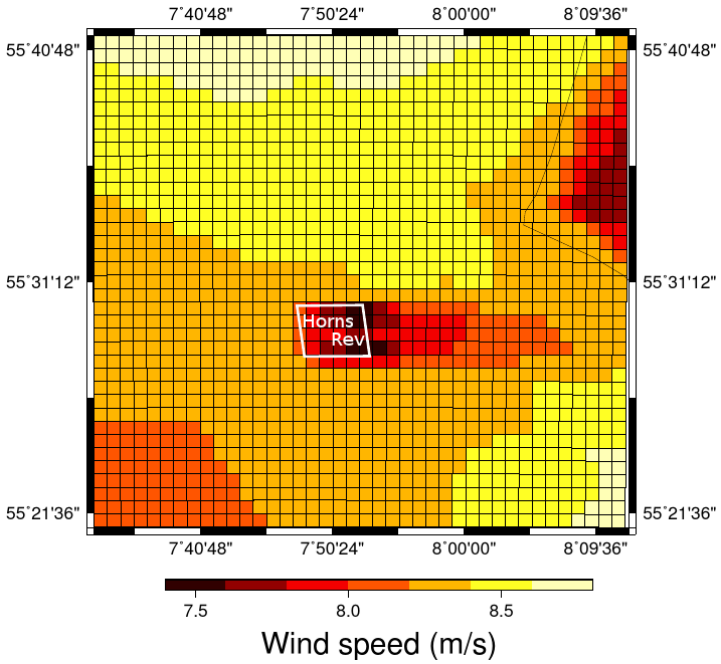

Figure 7: Maps showing the mean wind speed averaged for those instants with neutral stratification and western winds.

The WRF model was configured with a total of 4 domains to progressively reach a horizontal resolution of 1 km in the innermost domain that covers the complete cluster (black dots in Figure 8). Although this resolution can be considered high for a mesoscale model we are not able to individually resolve all the wind turbines, some of them being collectively modelled. Two numerical experiments were performed. The first one does not activate the wind farm parameterization (hereafter referred to as WRF*default*) so the influence of the wind farms over the atmospheric flow is not considered. The second experiment activates the parameterization (hereafter referred to as WRF*cluster*) of the effects of the wind turbines but does not include the wind turbines of the reference wind farm (Figure 8). By comparing results from both WRF runs we are able to discern any potential influence of the wind farm wakes over the target location, the reference wind farm. A real case with western winds spanning one day was selected for study.

The modelled wind direction at the reference wind farm (blue cross in Figure 8) is shown in Figure 9. Both simulations WRF-default and WRF-cluster show a similar temporal evolution. The winds are from the northwest during the first 12 hours of the simulation when the flow starts to veer to the west-southwest. This different evolution of the flow shows profound implications for the wind speed at the reference wind farm (Figure 10). The first half of the day both WRF runs show similar values since there are not wind farms to the northwest of the reference wind farm (Figure 8). However, during the second half of the day, the winds are from the west and there is a big impact in the wind speed in the simulations. WRF-cluster shows a reduction of the wind speed of a few m/s. Wind speed deficits of this magnitude has been observed at large offshore wind farms using satellite data (See section 7). This indicates that the reference wind farm will show a reduction of the power production as a result of the wakes from the surrounding turbines. A more detailed analysis including observations over the region should be accomplished to complement this modelling result.

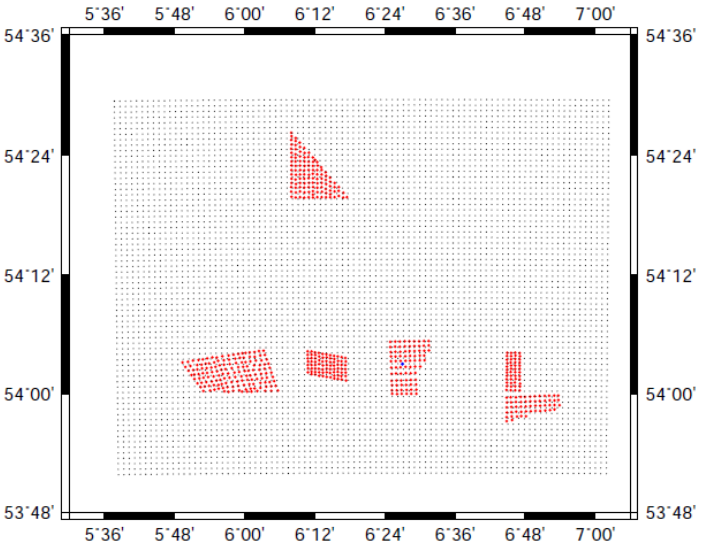

Figure 8: Set up of large cluster of wind farms modelled within WRF. The red dots indicate the location of future wind turbines whereas the black dots are the grid points of the WRF innermost domain configured at 1 km horizontal resolution. The blue cross denotes the location of a site within the reference wind farm.

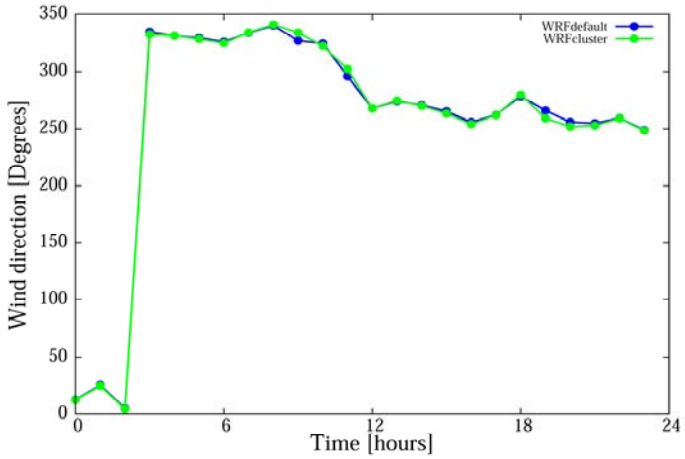

Figure 9: Modelled wind direction at the reference wind farm (blue cross in Figure 8) with WRF-default (blue) and WRF-cluster (green).

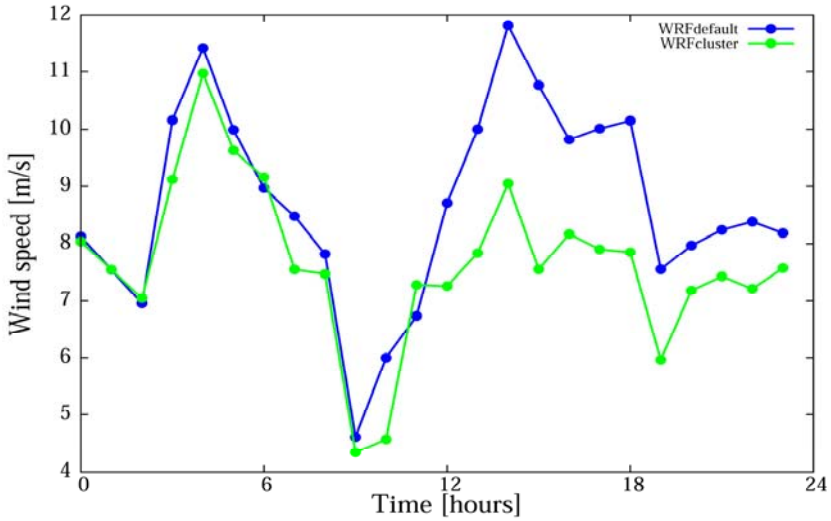

Figure 10: Same as Figure 9 but for the wind speed.

6 CENER METHODOLOGY:

With the goal of simulating the wake effects produced by a large offshore wind farm, or a wind farm cluster in the surrounding area, CENER purposes an approach based on mesoscale numerical model with a wind farm equivalent 'added roughness'.

The most important challenge when applying a numerical mesoscale model to resolve the flow dynamics of large wind farm clusters is the representation of wind turbines/wind farms within the model (Frandsen et al., 2009). A baseline approach to simulate wake effects produced by a wind farm is to change land-surface properties. This means depicting the area of the offshore wind farm as an area of higher roughness than the sea surface.

CENER's methodology consists of two steps:

1 – Perform a long term simulation using a state of the art mesoscale model (SKIRON) to obtain the wind climatology of the region, which is used as reference. It represents the closest representation of the state of the atmosphere and it is a conventional approach in preliminary wind resource assessment studies where wind farm effects are not considered. This methodology has been validated in various studies (Cantero et al., 2011).

This reference wind map can also be used as input to microscale models, since it will be possible to obtain a long term wind time series or a vertical wind profile from every grid point of the model.

2 – Change the land use of the mesoscale model, to a value representing an "offshore wind farm class" and calculate a new modified wind resource map by simulating a typical year, representative of the long term climatology of the region (Chávez et al., 2013).

Once we have the two wind atlas, "standard" and "modified", the wake effects can be obtained by comparing both mean wind speeds at every grid point of the model and a wind/power deficit can be obtained at every point of the simulated domain.

The wind speed deficit is:

$$WspeedDeficit = \frac{(U - U_0)}{U}$$

where U is the simulated wind speed without the presence of wind farms, and U_0 is the simulated wind speed taking into account the Wind farm layouts.

To test the sensitivity of current state of the art mesoscale models, the Horns Rev wind farm is simulated with WRF and SKIRON models and the results are validated against the measurements provided by the EERA-DTOC project.

At the same time, a set of virtual offshore wind farm layouts Figure 13 are simulated with SKIRON at 5km resolution in order to test the response of the model when the roughness of a few domain's cells are changed. These experiments allow us to get a testing scenario to study farm-farm interactions.

6.1 Skiron Model Configuration:

CENER uses the SKIRON model to perform long term simulations. The regional weather forecasting system SKIRON was developed for operational use at the Hellenic National Meteorological Service. The physics options used are the Betts-Miller- Janjic convection scheme, Ferrier microphysics scheme, Lacis and Hansen shortwave radiation scheme, Fels and Schwarzkopf long wave radiation scheme, Noah land surface scheme, Mellor-Yamada 2.5 turbulence scheme and PBL, with Monin-Obukhov similarity theory in the surface layer and Paulson stability functions Kallos et al (2005).

The SKIRON model domain (Figure 11) is configured with a horizontal resolution of 0.05x0.05 degrees (approximately 5 km resolution) and 50 vertical levels generating outputs every hour Lozanu et al (2009). A period of 10 years was simulated (June 2003 to May 2013) using the GFS 12 UTC data as input.

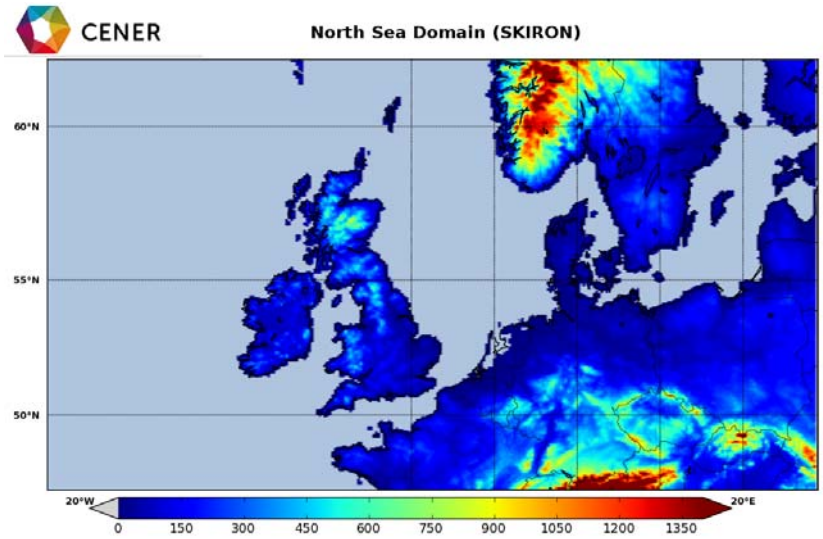

Figure 11: SKIRON Domain to the North Sea region (0.05x0.05 degrees resolution)

The offshore mean wind velocity for the 10-year period, at 80 m, is presented in Figure 12.

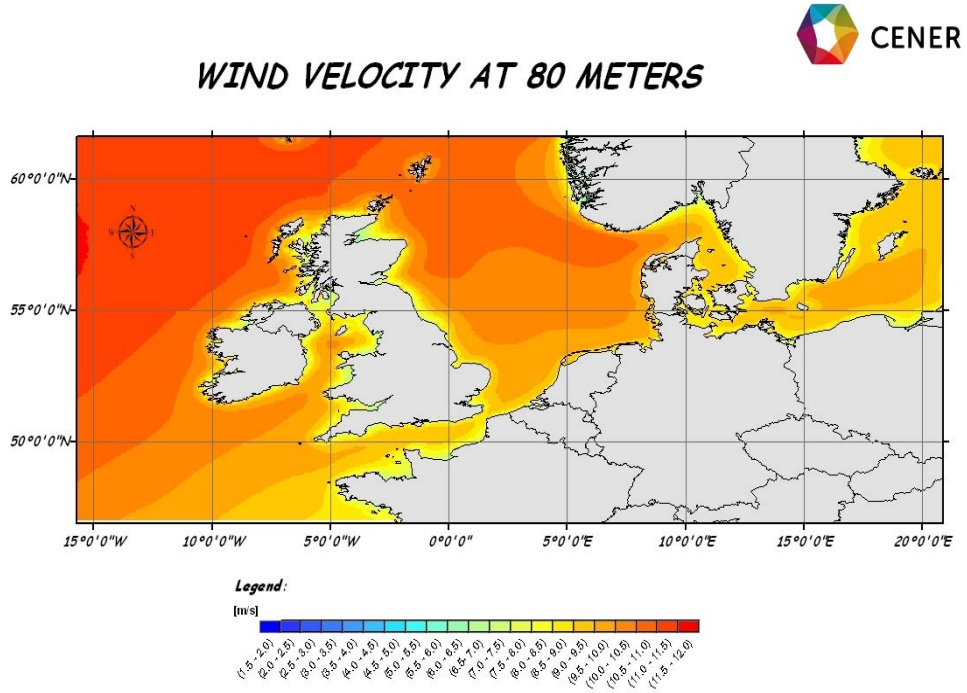

Figure 12: North Sea Offshore Wind Map, showing mean wind speed at 80 m above surface level, obtained with SKIRON (10 years period)

A second simulation is performed using the same domain and physical configurations, but using a different land use to reflect several virtual wind farm layouts, including Horns Rev as the only real wind farm layout. Two 1-month periods are simulated, January and July 2006, to represent respectively winter and summer climatology. The different wind farm layouts were placed at a sufficient distance from each other, so that the produced wakes won't affect the other layouts.

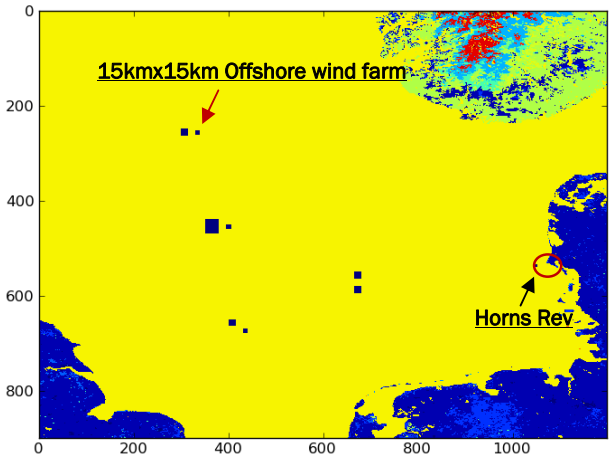

Figure 13: Wind Farm Layouts for the SKIRON wind farm cluster test case

6.2 WRF Model Configuration:

The model was centred at the Horns Rev wind farm, using four two-way nested domains with resolutions ranging from 16.2 km in the outermost domain to 600 m in the innermost domain Figure 14.

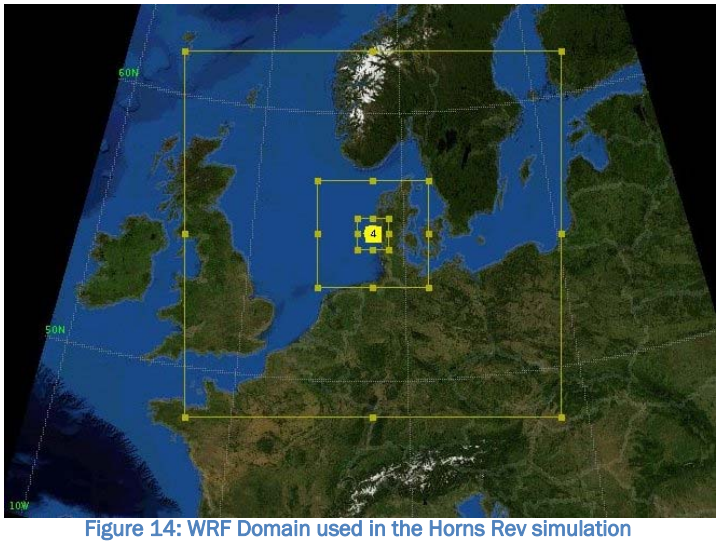

Figure 14: WRF Domain used in the Horns Rev simulation

The domain has 50 vertical levels and the following parameterizations were used: WRF Single-Moment (WSM) 3-class simple ice scheme, RRTM scheme, Dudhia scheme, Monin-Obukhov Similarity scheme, Thermal Diffusion scheme and YSU scheme.

6.3 Mesoscale model sensitivity test:

6.3.1 WRF-ARW

A test case, using the HornsRev offshore wind farm layout, is performed. Using the WRF-ARW version 3.3 mesoscale model, one day (23-06-2013 12:00 until 24-06-2013 15:00, and the first three hours of simulation were discarded) was simulated applying a modified land use database (same roughness as a city) including the HornsRev wind farm layout, Figure 15.

The main goal is to test the sensitivity of the current NWP models to simulate wake effects based on a roughness change and ascertain the effect of that wake in the surrounding region.

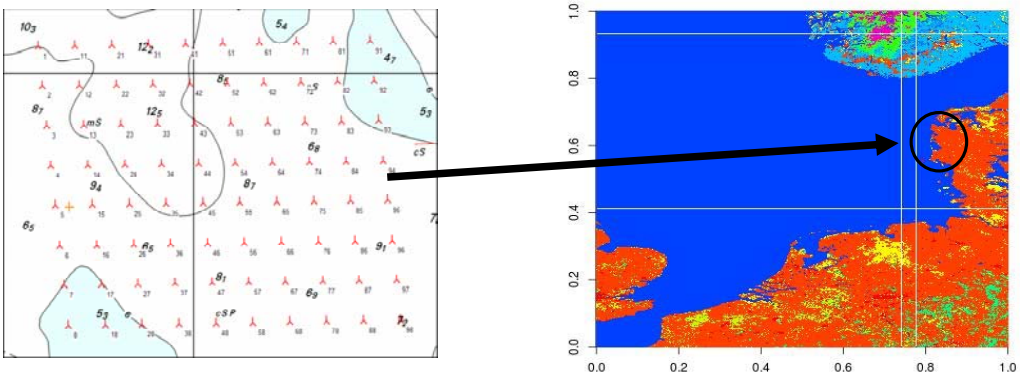

Figure 15: Modified Land Use, including Horns Rev Wind Farm

The results show that the WRF model is able to detect the presence of the wind farm and a significant velocity deficit is clearly noticeable, Figure 16.

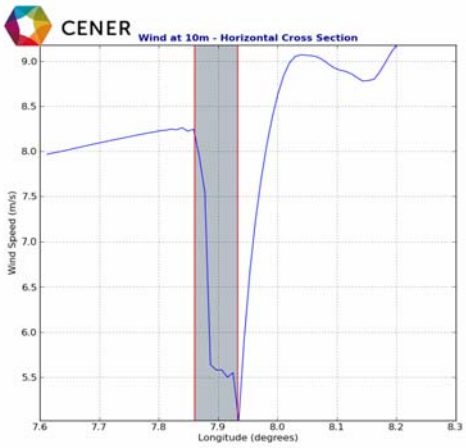

Figure 16: 10 m wind speed at a horizontal cross section that passes through the center of Horns Rev Wind Farm

In order to proper validate the results of the simulation, all the wind speeds are normalized. In addition, the predicted wind speeds are classified for different wind direction sectors, taking into account the predicted wind direction at the reference tower “M2”. The wind speed deficit is shown in Table 3.

Even with this very simplistic approach, the results indicate that wind speed deficit errors are below 10%, which means that current methodology can provide useful information in the initial stages of wind farm planning.

Sector	Positions	Speed Meas. (%)	Speed WRF (%)	Error (%)
252.5-257.5	M2-M6	13.6	12.32	-1,28
	M2-M7	6.05	4.98	-1,07
257.5-262.5	M2-M6	11.54	11.57	0,03
	M2-M7	3.76	3.69	-0,07
262.5-267.5	M2-M6	16.05	11.73	-4,32
	M2-M7	9.88	3.56	-6,32
267.5-272.5	M2-M6	13.06	10.54	-2,52
	M2-M7	8.32	4.92	-3,40
272.5-277.5	M2-M6	13.74	15.12	1,38
	M2-M7	9.24	2.28	-6,96
277.5-282.5	M2-M6	14.27	5.54	-8,73
	M2-M7	4.63	-0.26	-4,89
282.5-287.5	M2-M6	11.84	16.42	4,58
	M2-M7	2.57	9.20	6,63

Table 3: Wind speed by direction sectors at Horns Rev Wind Farm

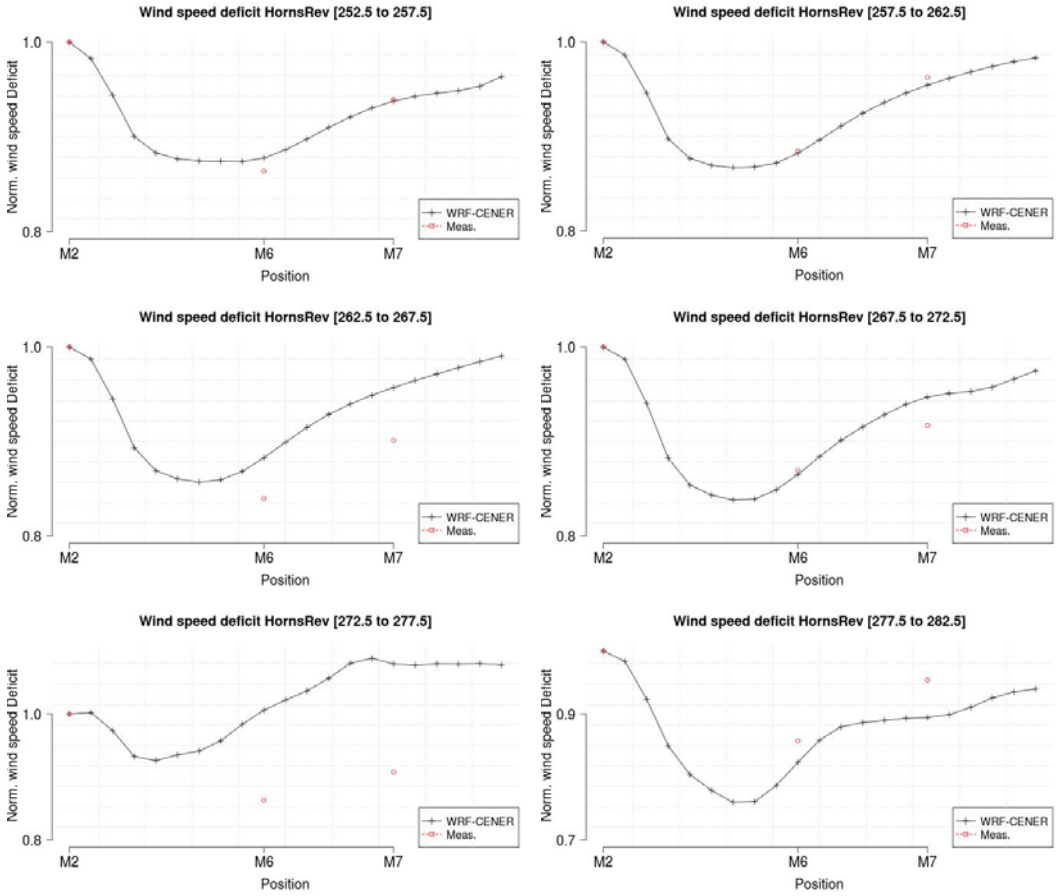

Figure 17: Normalized wind speed for six direction sectors at Horns Rev Wind Farm, WRF results against measurements.

6.3.2 Horns Rev Results by sector

Using the normalized measurements and predictions, 6 sectors are analyzed and the longitudinal profiles of wind speed deficit are presented in Figure 17 together with the met mast measurements located in the recovery region behind the wind farm.

With the exception of the sector 272.5º to 277.5º, the predicted wind speed deficit follows the same trend than the measurements. The higher differences observed in some sectors can be the result of a deficient wind farm layout representation by the WRF model, since the modified land cover doesn't represent the exact layout of the wind farm, Figure 18.

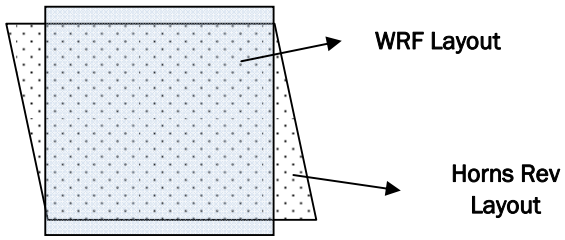

Figure 18: Difference between WRF and the real Horns Rev layout

Another source of error, probably the most important, is the short period that was simulated (only one day), which results in few samples for each sector of direction.

Further analysis will include longer model integrations to account for the wind climate variability throughout a typical year and obtain a representative value of the wind conditions affected by neighboring wind farms for every wind direction sector [1] and validate the results against all possible sectors.

6.3.3 SKIRON

The same land cover is used by SKIRON, but since the horizontal resolution in the simulation is only 5km x 5km, only the results at the wake recovery (M6 and M7) will be validated. Table 5 shows the normalized wind speed deficit at the Horns Rev wind farm.
The errors at the M6 tower are higher than at the M7 tower. Since the domain resolution is closer to the wind farm length, the model cannot detect the near wakes produced by the wind farm and only detects a slightly decrease in velocity. At the M7 tower the errors are lower than 8%.

6.4 SKIRON Test Cases

A simulation was performed with SKIRON using a modified land cover representing offshore wind farms Figure 13. Due to the SKIRON natural projection, the "real" wind farms are represented in the model as indicated in Figure 19. The normalized average wind speeds for the four wind farms are given in Figure 20.

It is possible to see that the model detects wind speed deficits when the land cover is changed into a different class with higher roughness. Farm 2, having the largest wind farm, reflects the highest deficit in wind speed. Since Farm 2 has the most significant changes, a more detailed analysis is presented. All the wind speeds are filtered by direction and divided into four sectors (North: 315-45; East: 45-135; South: 135-225 and West: 225-315).

Even though the SKIRON domain is configured with a relatively low resolution, it seems that the predicted wakes are still detected at very high distances from the wind farms.

	M2		M6			M7		
Sector	WRF	MEAS	WRF	MEAS	ERROR (%)	WRF	MEAS	ERROR (%)
252,5-257,5	1,00	1,00	0,88	0,86	1,57	0,94	0,94	0,35
257,5-262,5	1,00	1,00	0,88	0,88	-0,27	0,96	0,96	-0,08
262,5-267,5	1,00	1,00	0,88	0,84	4,89	0,96	0,90	6,56
267,5-272,5	1,00	1,00	0,86	0,87	-0,52	0,95	0,92	3,58
272,5-277,5	1,00	1,00	1,01	0,86	14,25	1,08	0,91	15,74
277,5-282,5	1,00	1,00	0,82	0,86	-4,16	0,90	0,95	-6,11

Table 4: Normalized wind speed by direction sectors at Horns Rev Wind Farm modeled by WRF.

	M2	M6			M7		
Sector	SKIRON/MEAS	SKIRON	MEAS	ERROR (%)	SKIRON	MEAS	ERROR (%)
252,5-257,5	1,00	0,95	0,86	8,60	0,92	0,94	-2,50
257,5-262,5	1,00	0,93	0,88	4,65	0,89	0,96	-7,99
262,5-267,5	1,00	0,95	0,84	11,40	0,92	0,90	1,97
267,5-272,5	1,00	0,94	0,87	7,94	0,91	0,92	-0,34
272,5-277,5	1,00	0,94	0,86	8,69	0,92	0,91	1,46
277,5-282,5	1,00	0,96	0,86	11,09	0,94	0,95	-1,32

Table 5: Normalized wind speed by direction sectors at Horns Rev Wind Farm modeled by SKIRON.

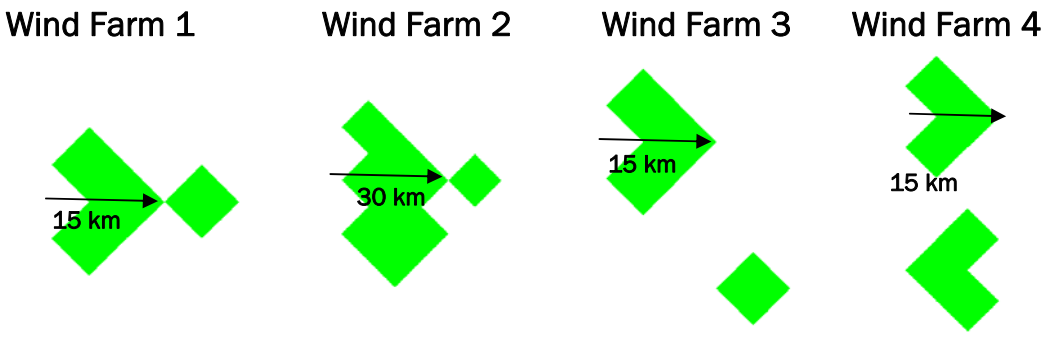

Figure 19: Wind farms within the SKIRON run with wind farm clusters, see Figure 13.

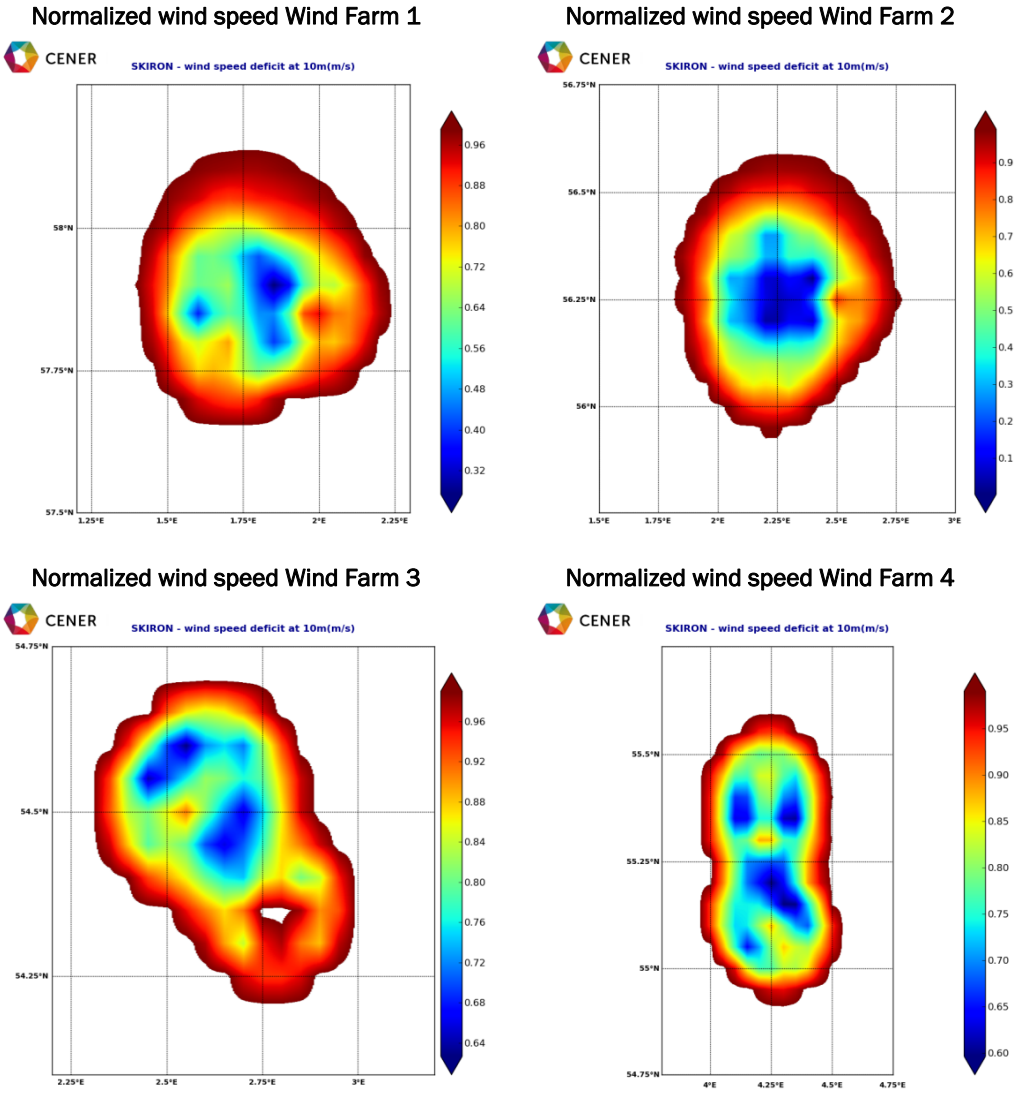

Figure 20: Average normalized wind speed to the 4 Test cases

North (315-45)

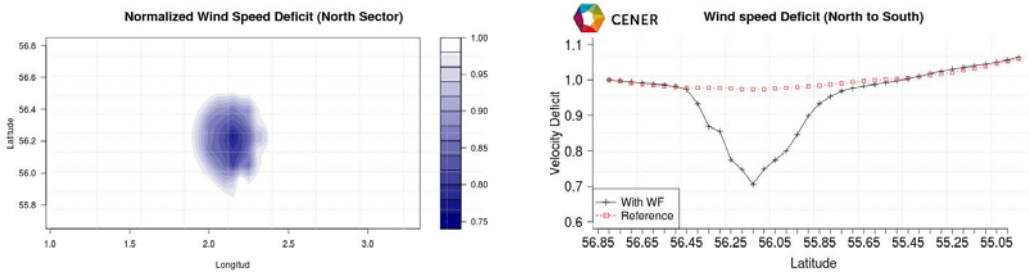

Figure 21 : Normalized wind speed in the wind farm region (left) and North-South cross section (right)

East (45-135)

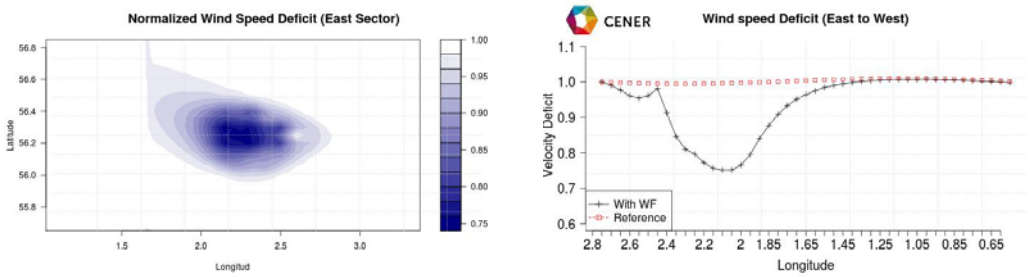

Figure 22: Normalized wind speed in the wind farm region (left) and East-West cross section (right)

South (135-225)

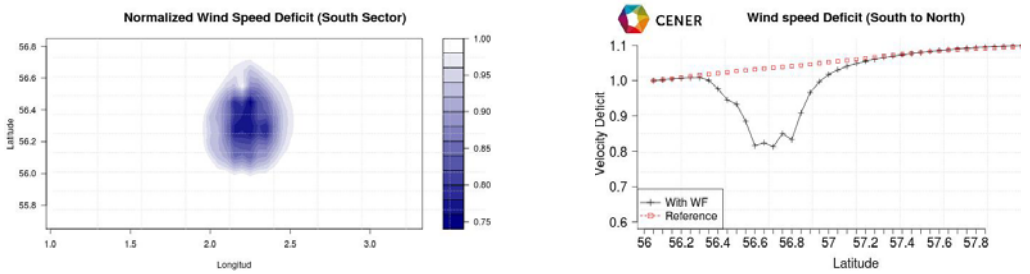

Figure 23: Normalized wind speed in the wind farm region (left) and South-North cross section (right)

West (225-315)

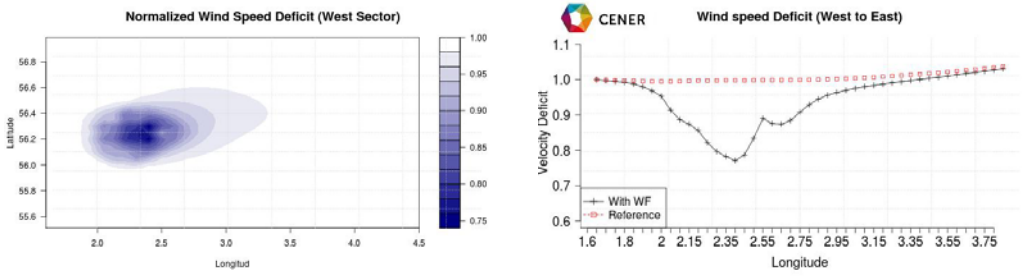

Figure 24: Normalized wind speed in the wind farm region (left) and West-East cross section (right)

7 CLS AND DTU WIND ENERGY – SATELLITE DATA ANALYSIS

Satellite SAR scenes have been collected at CLS and DTU for the quantification of wind farm wakes. The satellite data analysis is divided in two parts:

1. Investigation of specific cases at different offshore wind farms. A series of 23 high-resolution scenes from the Radarsat-2 mission are used for this; more details can be found in report **D1.1 Basic data for testing of mesoscale and coupled use**. Results of this analysis are described in section 7.1 and 7.2.

2. Investigation of the mean wind speed around the offshore wind farms Horns Rev 1 and 2. Lower-resolution (150 m) Envisat ASAR data acquired in Wide Swath Mode (WSM) are held in archives at both CLS and DTU. These data archives are combined to achieve the highest possible number of samples over Horns Rev. Results of this analysis are described in section 7.3.

For both of the analyses, wind speeds at the 10-m level have been retrieved from each SAR scene by CLS. The wind speed is a function of the Normalized Radar Cross Section (NRCS), the wind direction relative to the radar look direction, and the radar incidence angle. The relationship of these parameters is given by an empirical Geophysical Model Function (GMF). The wind direction input, which is required to retrieve the wind speed, is from the European Centre for Medium-Range Weather Forecasts (ECMWF) model. See Hasager et al. (2012) and http://soprano.cls.fr (winds, observations (L2)) for further details about the processing chain for the ocean wind field retrieval.

7.1 Visual indications of wakes (qualitative), including identification of meandering.

The whole archive available at CLS has been manually investigated to select the most relevant wind wakes signature in high resolution radar image. This work is still going on as Radarsat-2 products are still routinely acquired by CLS VIGISAT receiving station located in Brest (France).

The strategy is as follow:

- All acquisitions are visually checked to detect any interesting features by Radar analysts.
- Interesting cases are analyzed in details to derive high resolution ocean surface wind fields.
- The most interesting cases are posted on CLS EODA (Earth Observation Data Access) web site. It aims at showing to all how wakes signatures on the ocean sea surface wind can be captured by high resolution radar imagery. Figure 25 presents the homepage of EODA and indicates the direct link to access the data. Access is free without any login or password. 23 radar images with wakes signature can be browsed.

The wind retrieval is based on the analysis of the backscattering intensity (or Normalized Radar Cross Section: NRCS) of the emitted radar wavelength by the sea surface small waves that directly respond to the surface wind. The backscattering from the sea may be disrupted by any oceanographic, atmospheric and/or human actions which will impact the sea surface small wind generated waves. Any offshore installations or ships also impact the NRCS as they have a strong backscattering echo (they are called “bright targets”). In North Sea, the traffic density is very high (with major navigation passes and large mooring areas) and many offshore installations are implanted. As a consequence the image intensity analysis to get wind measurement at high resolution has to be adapted to efficiently filter out artefacts.

Figure 25: EODA homepage to get access to radar images where significant wakes signatures have been observed from space, https://eoda.cls.fr .

The detection of bright targets is based on their likely higher radar cross section (RCS) with respect to the sea surface. This scheme assumes a high RCS from targets such as vessels and a low RCS from sea. For low-to-medium resolution SAR imagery (above 20 meter resolution), target detection is generally carried out by adaptive threshold using a sliding window. The most common approach is the Constant False Alarm Rate (CFAR) methodology usually applied on a pixel-basis.

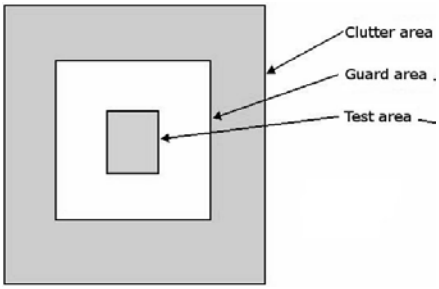

Figure 26: Typical CFAR windows

CFAR-based methodologies are based on a pre-determined false alarm rate which is then used to compute the appropriate threshold given a probability density function for the clutter (Gaussian, Gamma or K-distribution). One basic method for CFAR detection would be to work directly with the histogram of the background windows and set the threshold at the appropriate point in the tail of the distribution. For operational purposes (computation efficiency), CFAR is generally based on the first two moments (average and variance). The sliding window is hence partitioned into three parts as illustrated by Figure 26. The cell under test is in the middle. The purpose of the guard area is to ensure no part of an extended target is included in the background area and hence the clutter area is representative of the background statistics. The dimensions of target, guard and background areas in pixels domain have to be adapted to image resolution in both range and azimuth directions, and to the minimal and maximal dimensions of the ship under consideration.

In the frame of this study aiming at generating high quality wind fields from SAR imaginary, the size of CFAR kernel and prior False Alarm Probability have been tuned so as to filter not only bright man-made target (vessels, oil/gas platforms) but also other metoceanic more-diffuse bright features (cell rains, very local oceanic fronts…). Once a specific bright echo is detected, a surrounding buffer area of 300 m is excluded when computing the kilometric quick-look intensity image used for wind inversion.

In addition, to date known wind farms areas are systematically rejected from the inversion process. Indeed for these very dense areas, the loss in detectability caused by the presence of one or more interfering target returns within the clutter area can be severe. However, some recent methodologies use a ranking and censoring technique that prescreens the clutter pixels [Gao et al. 2009]. Investigations to apply these techniques to our wind inversion scheme will be carried out in the future.
Furthermore, in the case of non-homogeneous or non-Gaussian clutter (in transition regions with different wind conditions or bathymetries), false alarm rates can increase. Both low and high resolution SAR images are concerned. In order to tackle these effects, a segmentation-based technique may be relevant to merge pixels with similar backscattering behaviour [Lombardo et al. 2001]. This is one perspective to improve our methodology.

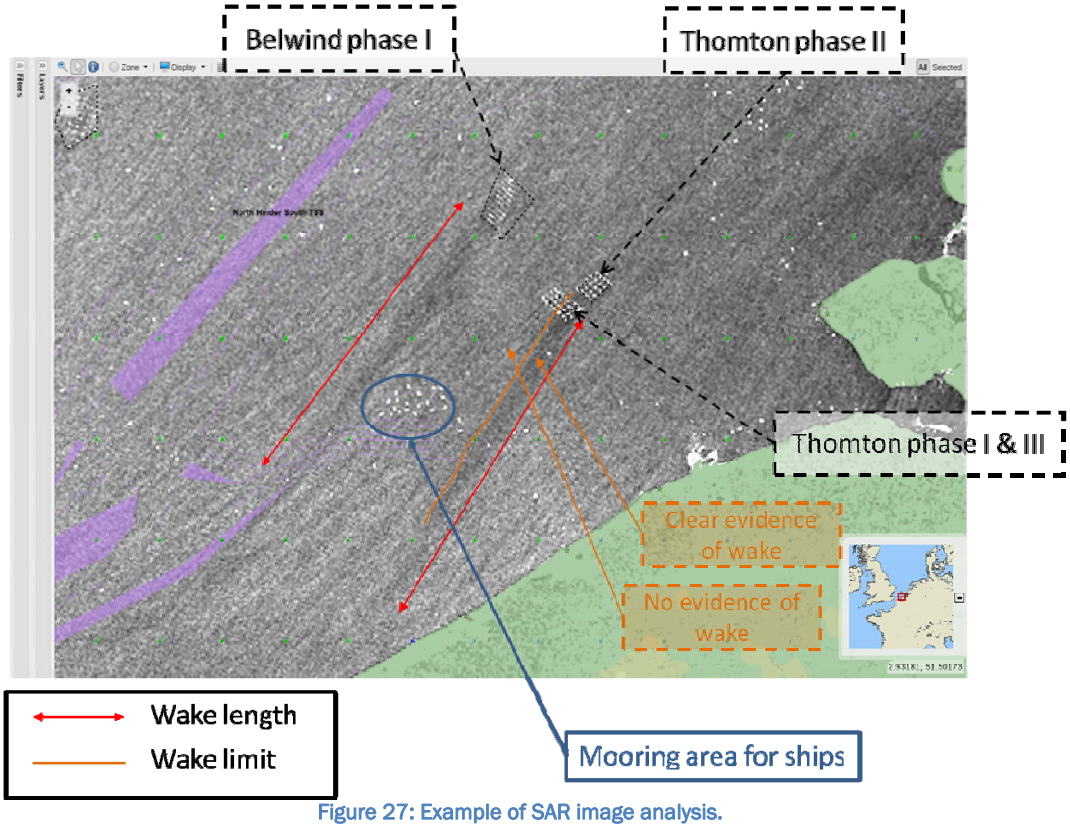

Figure 27: Example of SAR image analysis.

An example of radar image analysis is shown in Figure 27. The NRCS intensities are normalized and range between 0 and 255. Bright points are strong echoes from ships and wind turbines. Dark areas indicate areas with low wind speed. When they are located behind wind farms they indicate local wake effects on the mesoscale wind flow.

The wind field measured from this measurement is shown in Figure 28. As observed the wind decreases behind wind farms.

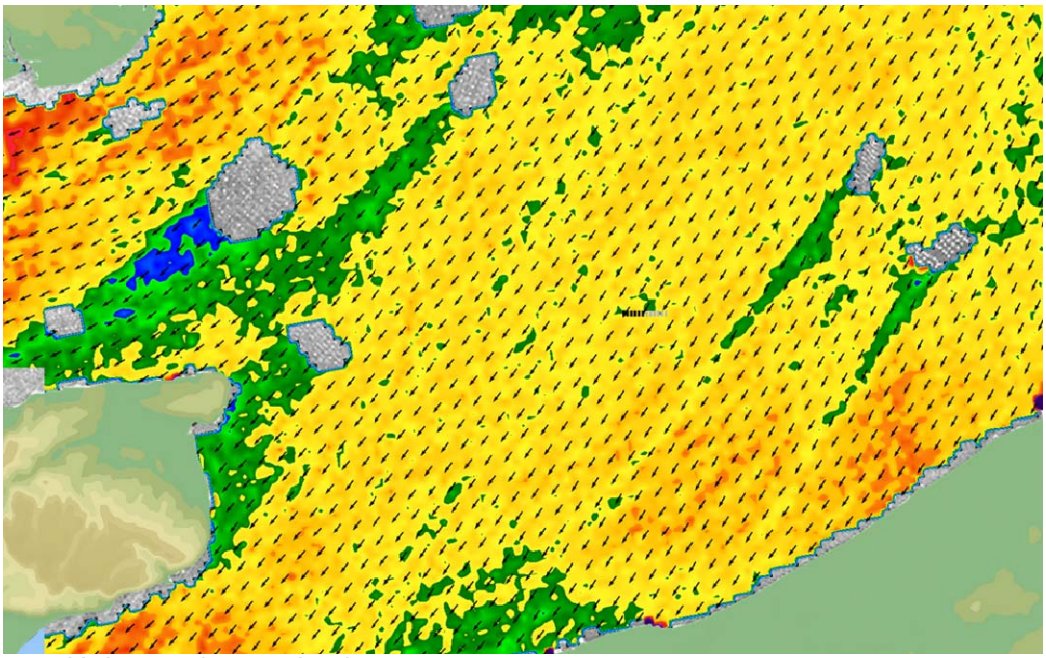

Figure 28: Ocean surface wind field from high resolution radar. We observe that behind Thomton, the wind field decreases from 9 to 7 m/s at the sea surface. In this case, wake seems to be larger and the decrease of wind higher for bigger wind farms (see London Array for instance)

7.2 Analysis of single scenes, using 3 parallel transects

The high resolution SAR scenes produced by CLS (described above) can be analyzed quantitatively with a method extending that used in Christiansen (2006) in order to determine properties of the wind farm wake. The method developed within DTOC is to analyze mean wind speed along three parallel transects aligned with the wind direction; one passing through the wind farm, and two passing to the left and right of the wind farm respectively. The transects passing to the left and right provide two non-disturbed flow references to compare to the wake influenced central transect.

Each transect is made up of a series of averaging boxes placed in a line. The size of the averaging boxes, the length of the transects and the transect separations were adapted for each of the cases. Four examples of the analysis are shown graphically in Figure 29 and Figure 30. For each case, a SAR derived wind speed map is shown with the central transect axis marked over it, note that the axis begins upstream of the wind farm, also shown is the averaging box composition of each of the transects. Then, two line graphs indicating i. the box averaged wind speed along the transects, and ii. the normalized wind speed within the wake are given. The normalized wind speed is calculated by dividing the central transect wind speed by the left and right transect wind speed at the same distance along the transect axis.

Figure 29 (a) and (b) show two drastically different kind of meteorological situations over Horn Rev and Robin Rigg respectively. In the first case there is a steadily increasing easterly wind (from 4 to over 8 m/s) as the distance to the Danish coast increases. The wake caused by Horns Rev II is visible and the transect analysis shows that the wake extends to around 80 km downwind of the wind farm. In the second case the wind field around Robin Rigg is more complex with mesoscale variability caused possibly by a combination of convection and orographic effects. Even in this case the transect analysis indicates the presence of a wind farm wake approximately 15 km downwind, indeed until the coast is reached.

Figure 30 (a) and (b) show for the same SAR scene analysis of the wakes from Horn Rev I and II respectively. In these cases the wind farm wakes extends to around 15 km and 25 km.

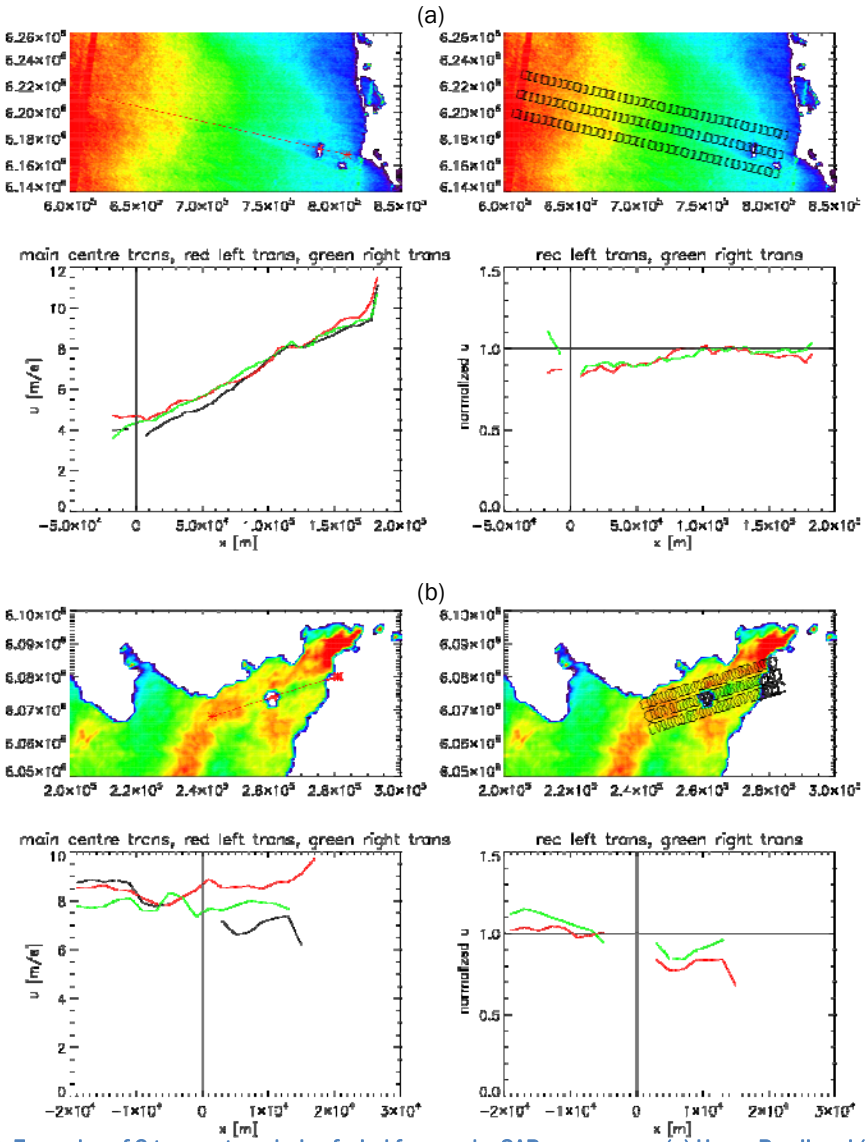

Figure 29: Examples of 3-transect analysis of wind farm wake SAR scenes over (a) Horns Rev II and (b) Robin Rigg. For (a) transect length is 200 km, separation 15 km, averaging box width 5 km and box length 5 km. For (b) transect length is 40 km, separation 4 km, averaging box width 2 km and box length 2 km.

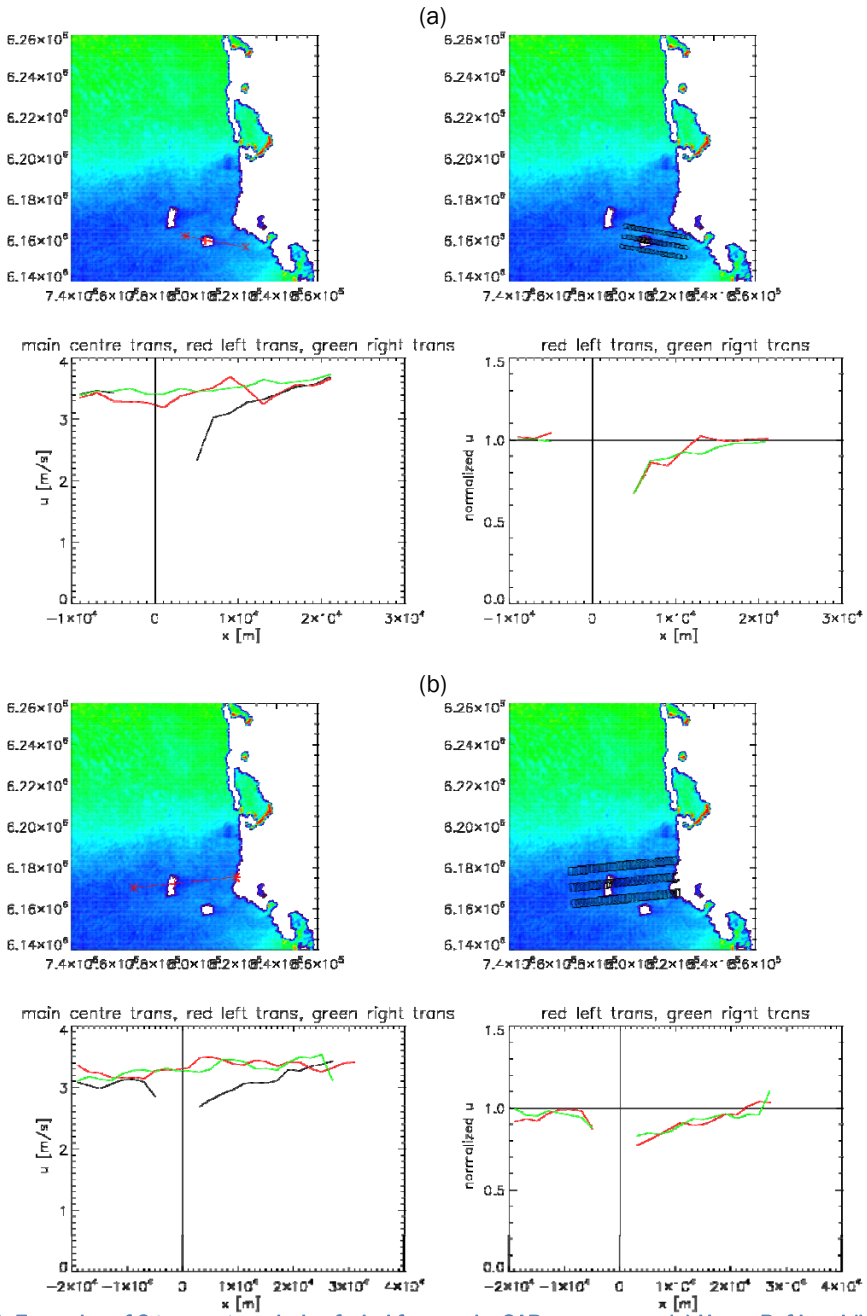

Figure 30: Examples of 3-transect analysis of wind farm wake SAR scenes over (a) Horns Ref I and (b) Horns Rev II. For (a) transect length is 40 km, separation 5 km, averaging box width 1 km and box length 1 km. For (b) transect length is 60 km, separation 8 km, averaging box width 2 km and box length 3 km.

7.3 Climatological (averaged) analysis of wind farm wakes.

A total of 923 wind fields retrieved from Envisat ASAR WSM scenes from 2002-12 are available over the two wind farms at Horns Rev. The wind fields cover a swath width of 400 km with variable lengths. The number of overlapping samples is therefore also variable across the area of interest. The spatial resolution of the wind fields is 1 km because pixels are averaged during the wind field retrieval. This is to reduce effects of random noise and ocean waves which have longer periods than the cm-scale waves that the SAR senses.

The SAR wind fields are filtered such that only samples with wind speeds in the interval 4-14 m s^{-1} at a point between Horns Rev 1 and 2 (7.75 E, 55.55 N) are used. The 740 samples, which fulfill this criterion, are distributed into 12 directional sectors based on the wind directions at the same point. Note that the wind directions originate from the ECMWF model, not the satellite observations. For each directional sector, the mean wind speed is calculated for the overlapping wind fields. Table 6 shows the number of overlapping scenes per sector.

Sector	0	1	2	3	4	5	6	7	8	9	10	11	Total
Degr. (± 15)	0	30	60	90	120	150	180	210	240	270	300	330	-
N	29	26	42	38	75	50	55	104	89	76	87	69	740

Table 6: Number of Envisat ASAR satellite samples (N) for 12 wind sectors

Figure 31 and Figure 32 show maps of the mean wind speed (U) for each of the 12 directional sectors normalized with the mean wind speed of a reference area (U_{ref}) where effects of the wind farms and the land are limited. Ratios of U/U_{ref} below 1.0 indicate that the wind speed is lower than the reference wind speed. Most of the maps show a reduction of the mean wind speed at the downwind side of the two wind farms. The effect can be difficult to distinguish from other effects, which cause spatial variability of the mean wind speed. For example, wind speed gradients near the coastline and signatures of bathymetry are seen on some of the maps. These effects have been described in more detail by Christiansen and Hasager (2003). In order to get a more quantitative estimate of the wake effect, a transect approach like the one described in section 7.2, will be followed.

The wind farm Horns Rev 2 became operational in the fall of 2009 so effects of this wind farm on the mean wind should be less evident than for the wind farm Horns Rev 1, which has been in operation since 2002 when Envisat was also launched. Horns Rev 1 is thus present throughout the SAR data series.

The wind farms Horns Rev 1 and 2 show values above 1.0 because scattering from the wind turbines cause a strong backscatter to the SAR, which is not related to the wind. This effect impacts the entire wind farm area and the maps can therefore not be used to describe the mean wind conditions between individual wind turbines.

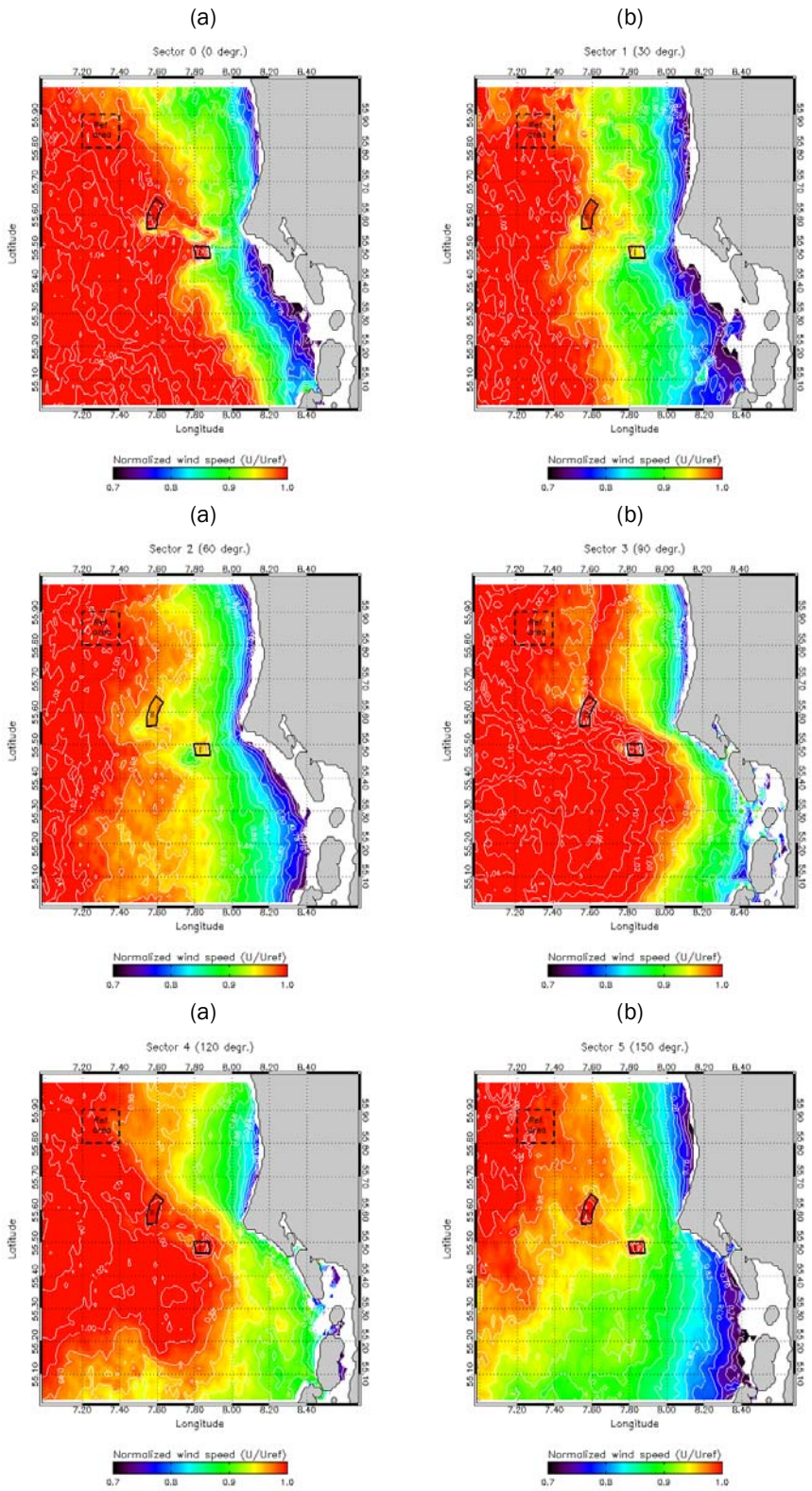

Figure 31: Maps showing the normalized wind speed for 30 degree direction sectors centred at (a) 0 (b) 30 (c) 60 (d) 90 (e) 120 (f) 150 degrees for an area around Horns Rev 1 and 2 wind farms based on wind fields retrieved from Envisat ASAR WSM (2002-2012)

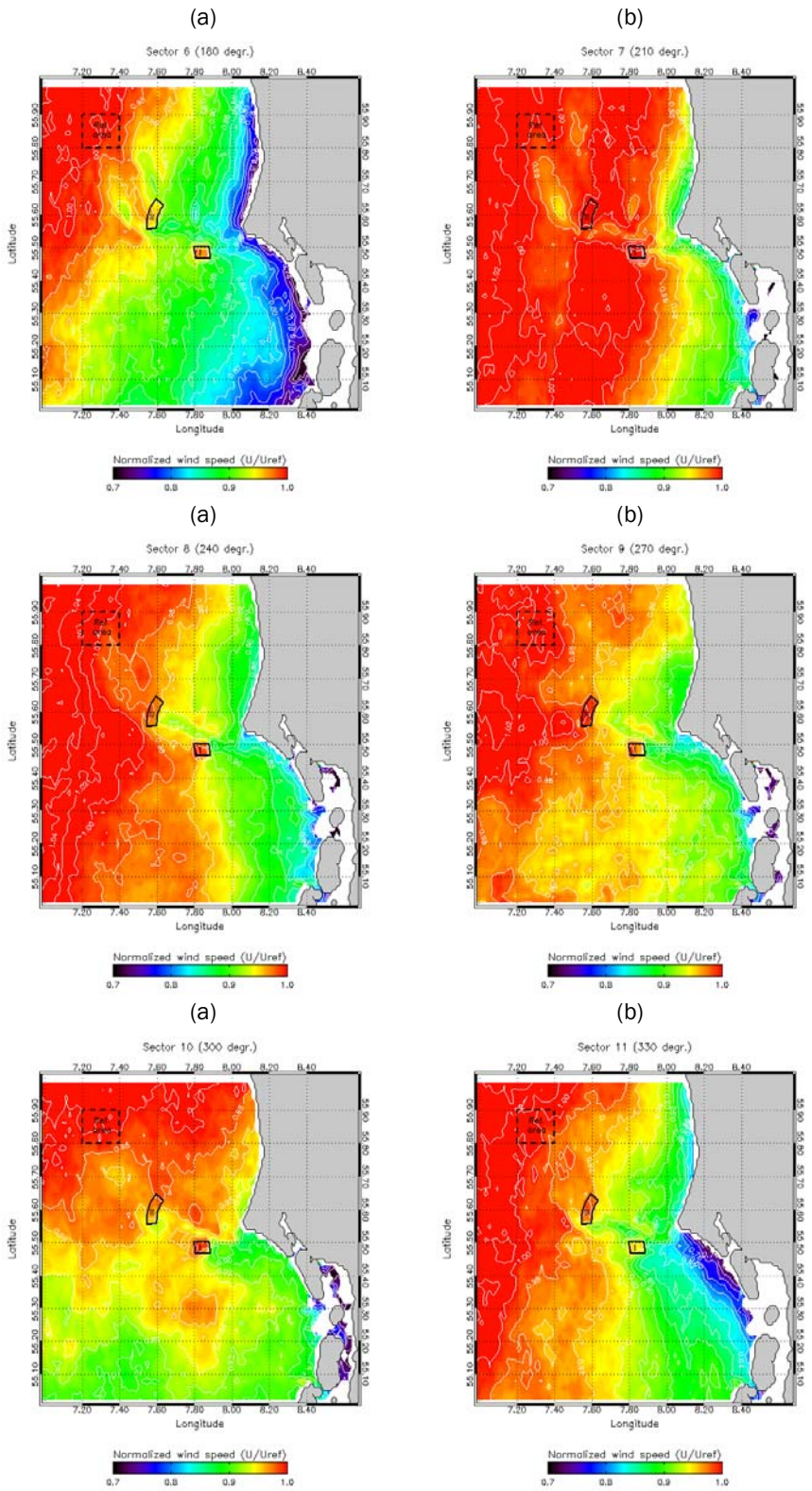

Figure 32: Maps showing the normalized wind speed for 30 degree direction sectors centred at (a) 180 (b) 210 (c) 240 (d) 270 (e) 300 (f) 330 degrees for an area around Horns Rev 1 and 2 wind farms based on wind fields retrieved from Envisat ASAR WSM (2002-2012)

8 SYNTHESIS AND DISCUSSION

In this section the various results described in this report are collected and compared across the different approaches. General characteristics of the results and approaches are summarized and consistency within the results is highlighted.

First, to an extent that is reasonably possible, the results of different approaches are collected for the Horn Rev I benchmarking data case 1 that consists of westerly winds and neutral atmospheric stratification (see D1.1 Basic data for testing of mesoscale and coupled use and Hansen, 2013).

		Normalized wind speed		
	Source	M6	M7	Notes
benchmarking data	Measurement	**0.83**	**0.91**	wind speed 8±0.5 m/s, direction 270 ±15 neutral Case 1 (Hansen, 2013)
microscale modelling	ECN FarmFlow 5 deg sector	0.92	0.93	as in case 1, with direction 270 ±2.5
	ECN FarmFlow 15 deg sector	0.90	0.93	as in case 1, with direction 270 ±7.5
	ECN FarmFlow 30 deg sector	0.88	0.93	as in case 1, with direction 270 ±15
mesoscale modelling	WRF-EWP	0.85	0.89	as in case 1, with direction 270 ±15,
	WRF-CRES-EWP	0.86	0.89	as in case 1, with direction 270 ±15
	WRF-CRES-ROTOR	0.80	0.87	as in case 1, with direction 270 ±15
	WRF-CRES-ROTOR-FA	0.84	0.91	as in case 1, with direction 270 ±15
	WRF-Fitch et al (2012)	0.95	0.96	as in case 1, with direction 270 ±5
	WRF-roughness	0.86	0.95	no wind speed filter, direction 270±2.5, based on single day's simulation
	SKIRON-roughness	0.94	0.91	no wind speed filter, direction 270±2.5, based on single day's simulation
	mean	*0.87*	*0.91*	
	s.d.	*0.05*	*0.03*	
SAR remote sensing	SAR scene	0.85	0.93	based on single SAR scene
	SAR climatology	0.91	0.91	wind speeds > 4 m/s, direction 270±15

Table 7: Table showing the results from the different approaches for the Horns Rev I wind farm masts M6 and M7 based on the benchmarking data case 1, D1.1 Basic data for testing of mesoscale and coupled use and Hansen (2013).

Table 7, shows the main results against the benchmarking measurement analysis (Hansen 2013, **D1.1 Basic data for testing of mesoscale and coupled use** and used in **D1.3 Benchmark report on wake models at wind farm scale**). When reading this table it is important to consider that not all the values can be directly compared due to different assumptions or filtering. However there is still value in seeing where there is broad agreement or where values do not agree.

The different approaches tend to underestimate the wind speed deficit at M6, and the results are in better agreement with observations at M7. It is interesting that the variance of the mesoscale modelling results at M6 is larger than at M7. This may be indicative of the difficulties modelling the relatively near mesoscale wake (<4 km) in comparison to the relatively far mesoscale wake (>4 km). This has been noted in the report in connection with the SKIRON simulations where wind farms are modelled with increased roughness length, and the resolutions was 5 km. Of note is that the mesoscale approaches provide similar results that the reference simulations from the microscale model.

In spite of the different ways the wind farms are represented in the mesoscale models (i.e. Volker et al. (2013), Fitch et al. (2012), and the method based on increasing surface roughness), broadly similar modeling results at more than 4 km downwind of the wind farms are found. Hence, the estimates of wind speed at M7 are less sensitive to the approach which is used. This is likely to be due to at least two issues, (1) resolution of the wind farm; the wind farm is represented at relatively low resolution, compared to farm dimension and (2) the representation of the wake in the mesoscale model in some way settles at a couple of grid points downwind of the wind farm, such that exact distribution (horizontal and vertical) of turbine thrust becomes less important with distance from wind farm. This is effect is seen when comparing the WRF-EWP and WRF-CRES-

ROTOR results for example. The WRF parameterization shows a weaker wind speed deficit partially associated with the representation of the thrust and power coefficients (see section 5)

Concerning the length of wakes, the work presented in this report has also highlighted that the extent of wind farm wakes modelled and measured by remote sensing ranges from 10 km to 80 km, depending on meteorological conditions. None of the results indicate that the length of wakes is exaggerated by one of the approaches.

There is a need to consolidate the conclusions regarding the different approaches using identical idealized and realistic (dynamical) modelling frameworks under quite different atmospheric conditions. Wind resource assessment including wind farm wake effects can be calculated using a large number of idealized simulations (based on the statistical dynamical downscale methodology developed at DTU Wind Energy), or could be calculated using a dynamical downscaling methodology like that used at CENER, CIEMAT and DTU Wind Energy. The choices required during the development of the DTOC tools need to evaluate the strengths of these different methodologies. For future work, it is proposed that the simulations for climatological studies that do not comprise a period of one year are extended to this temporal coverage or more

Coupling mesoscale to microscale will also be an area of future work. It includes consideration and seeking solutions to determining what microscale models can utilize from the mesoscale models and defining how data is input into the microscale models. Information of interest includes inflow and in-wind farm vertical profiles of wind speed wind direction and temperature, wind speed and direction distributions, spatial and temporal variability of wind speed and direction, roughness of the ocean surface, or information of the turbulent state.

Extension of the already started work on extracting relevant information from microscale models to mesoscale model wind farm wake parameterization is also to be continued. The possibility of using different microscale model data for the mesoscale wind farm wake parameterization is the first step to be taken.

9 SUMMARY AND CONCLUSIONS

The model FarmFlow demonstrated that microscale models can be extended to calculate wake effects at the mesoscale. The WRF mesoscale simulations carried out within an idealized framework using the newly developed wind farm wake parameterization (WRF-EWP, Volker et al, 2013) have allowed for a close examination of the behaviour of the model and a validation against analysed measurement data. The WRF mesoscale simulation carried out within a realistic dynamical downscaling framework over the period of the Horns Rev I measurement data, using the implemented WRF (Fitch et al., 2012) scheme, has allowed for a validation against measurement data. It has also allowed for analysis of dynamic effects associated with changes in wind direction, whereby a wind farm wake from one wind farm can rather suddenly impact another downstream wind farm. This is likely to have an impact on the variability of the wind speeds at wind farms exposed to this effect. The mesoscale models SKIRON and WRF have been used to model wind farm wakes using increased surface roughness to represent the wind farms. Comparison has been made between the model results and data from Horns Rev I. SKIRON has been used to determine the climatological effects of large scale clusters of wind farms in the North Sea.

Studies using remote sensing data from satellite borne synthetic aperture radar (SAR) derived wind speeds have shown this data's potential for visual inspection of wake, transect analysis, and sectorwise climatological analysis. The data is highly valuable in providing spatial coverage of the wind speed field on scales appropriate for mesoscale modelling. Hence, it is an important data source to validate the ability of our parameterizations to reproduce the characteristics of the wakes related to large offshore wind farms.

This last point highlights an important aspect concerning validation of the modelling efforts. Since there are not yet enough measurements for performing a more thorough validation, across a large range of meteorological conditions, there is some uncertainty about the model results. The initial sensitivity test suggests that current mesoscale models can be used to simulate far wake effects of offshore wind farms. By simulating different offshore large wind farm or wind farm clusters surrounding the area of interest, it is possible to get a more realistic wind resource assessment study taking into account the effects of those wind farms on the area of interest.

It is recommended that more comparisons with observational datasets are carried out. The Lillgrund case could be used to perform a similar test of approaches, although this case lacks measurement covering the mesoscale (1 – 30 km). There is the possibility of using data from Fino 1, measurements impacted by wind farms in the vicinity. A closer work with industry will facilitate the access to more observations at existing offshore wind farms which would be of benefit for both the applied and the more academic research. Measurement data that allows for investigation of boundary layer stability effects, effects of inversion height will be of particular interest for the next steps in mesoscale wind farm wake modelling. In this direction, it looks very promising the prospect of data from the LIDAR measurement campaign associated with DTOC. This will be particularly of interest as it will cover some of the scales relevant for mesoscale modelling and collect high profile data.

Finally, it is recommend that the dynamical impact of wind farm wakes moving onto neighbouring downstream wind farms, at a shift in wind direction, is investigated further, as the possibility of added variability of wind farm production needs to be considered together with its implications.

10 REFERENCES:

Cantero, E., U. Irigoyen, P.Correia, L. Frias, Y. Loureiro, S. Lozano, E.Pascal, D.Cabezon, 2011, Cener Wind resources map and virtual maps at mesoscale: Onshore (Tunisia) and Offshore(Great Lakes), European Wind Energy Conference, Brussels

Chávez, R., Lozano, S., Correia, P., Probst, O.,2013, On the application of two statistical methods for an efficient climate downscaling of surface wind fields , Submitted to European Geosciences Union General Assembly 2013

Christiansen, M., 2006. Wind energy applications of synthetic aperture radar. PhD thesis. Risø National Laboratory. (Risø-PhD; No. 27(EN)).

Crespo, A., Manuel, F., Moreno, D., Fraga, E. and Hernández, J., 1985. "Numerical Analysis of wind turbine wakes". In Proceedings of Delphi Workshop on "Wind turbine applications"

Dee DP, Uppala SM, Simmons AJ, Berrisford P, Poli P, Kobayashi S, Andrae U, Balmaseda MA, Balsamo G, Bauer, 2011. The ERA-Interim reanalysis: configuration and performance of the data assimilation system. Quarter. J. Roy. Met. Soc.; 137:553597.

Fitch, A. C., Olson JB, Lundquist JK, Dudhia J, Gupta AK, Michalakes J, Barstad I., 2012. Local and mesoscale impacts of wind farms as parameterized in a mesoscale NWP model. Mon. Wea. Rev.; 140:3017-3038.

Frandsen, ST, Ejsing Jørgensen, H, Barthelmie, RJ, Rathmann, O, Badger, J, Hansen, KS, Ott, S, Rethore, P-EM, Larsen, SE & Jensen, LE, 2009, 'The Making of a Second-generation Wind Farm Efficiency Model Complex' Wind Energy, vol 12, no. 5, pp. 445-458.

Hansen, K. S., 2013: WP1 wake model performance validation results for Horns Rev offshore wind farm, 24 pp.

Jimenez, PA, J Navarro, AM Palomares and J. Dudhia, 2013: Mesoscale modeling of offshore wind turbine wakes at the wind farm scale. *Wind Energy* (Under review).

Kallos, G., Katsafados, P., Papadopoulos, A., 2005, *The weather forecasting system SKIRON: Description of the model*, University of Athens, 165pp

Lozano, S., U. Irigoyen, I.Martí, E. Cantero, E.Pascal, P. Correia, L. Frias, J. Garciandia, E. Zubillaga, *Wind resources map of Iberian Peninsula, using a mesoescale model. Comparison of different methodologies*, European Wind Energy Conference, Marseille, 2009

Panofsky, H and J. Dutton, 1984. "Atmospheric Turbulence". John Wiley and Sons..

Skamarock WC, Klemp JB, Dudhia J, Gill DO, Barker DM, Duda M, Huang XY, Wang W, Powers JG. 2008. A description of the advanced research WRF version 3. Technical Report TN-475+STR, NCAR.

Volker, P, J. Badger, A. N. Hahmann, S. Ott, 2013. Implementation and evaluation of a wind farm parametrisation in a mesoscale model, submitted to Boundary-Layer Meteorology.